2842817

This is to certify that the

thesis entitled

Fatigue of ThO_2 Dispersion Strengthened

Nickel Alloy with Surface Modification by Al^+ Ion Implantation

presented by

Robin Banerjee

has been accepted towards fulfillment
of the requirements for

M.S. degree in Materials Science

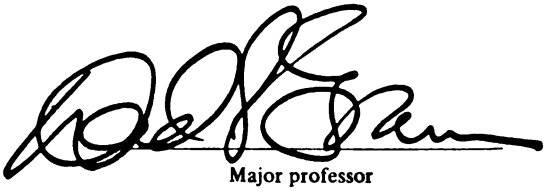

Major professor

(Dr. David S. Grummon)

Date May 17, 1989

FATIGUE OF ThO_2 DISPERSION STRENGTHENED NICKEL ALLOY WITH SURFACE MODIFICATION BY Al^+ ION IMPLANTATION

By

Robin Banerjee

A THESIS

Submitted to
Michigan State University
in partial fulfillment of the requirements
for the degree of

MASTER OF SCIENCE

Department of Metallurgy, Mechanics and Materials Science

1989

ABSTRACT

FATIGUE OF ThO_2 DISPERSION STRENGTHENED NICKEL ALLOY WITH SURFACE MODIFICATION BY Al^+ ION IMPLANTATION

By

Robin Banerjee

The present work was carried out to characterise the effects of high-energy ion implantation on the fatigue behavior of dispersion-strengthened (DS) nickel alloy. Direct Al^+ ion implantation was used to modify the surfaces of thoria-dispersed nickel alloy specimens. The fatigue behavior of both the unmodified and modified specimens was characterised in terms of cyclic stress-strain (CSS) response and by determination of low-cycle fatigue life in stress controlled tests. The surface modified specimens showed moderate increase in cyclic saturation stress as well as slightly improved low-cycle fatigue life. The unmodified specimens developed persistent slip bands (PSB) during fatigue and cracks initiated at the PSB-matrix interface. Surface modification by ion implantation was found to suppress and delay the formation of persistent slip bands and thus delayed crack initiation, resulting in higher fatigue life.

Dedicated to my parents

ACKNOWLEDGEMENTS

I would like to express my sincere thanks and regards to my advisor Dr. David S. Grummon for his continued support and guidance throughout the length of this project. Also thanks are due to Dr. L.T. Drzal and Mr. Michael Rich of Composite Materials and Structures Center, Michigan State University, and to Dr. Gary Was of Michigan Ion Beam Laboratory, University of Michigan, for provision of various facilities used in this work. Finally, special thanks are due to Sherritt Gordon Mines Ltd. for providing the material, and to the National Science Foundation for their financial support under grant #MSM807774.

TABLE OF CONTENTS

LIST OF TABLES

LIST OF FIGURES

CHAPTER I

INTRODUCTION

In recent years, high-energy ion-implantation has been succesfully used to improve surface-sensitive properties e.g, wear resistance and corrosion resistance of various materials. This process is now being investigated as a viable means to improve the fatigue performance of structural materials. Different combinations of implant and substrate materials e.g, Al implantation in Cu [Kujore, 1980], C implantation in Ni [Sleeswyk, 1980], Ne implantation in Cu [Bakhru, 1981], C and N implantation in Ti-6Al-4V alloy [Vardiman, 1982], Al implantation in Ni [Ahmed,1985; Grummon,1987; Jones,1987] have all resulted in improved fatigue life of the substrate materials. Various other combinations have also been found to produce fatigue life improvement [Mendez,1982; Jata,1983; Hohmuth,1985]. While ion implantation, in general, leads to higher fatigue life of target materials, it has been found in some instances e.g, C implantation in Cu and stainless steel [Sleeswyk,1980], to decrease the fatigue life. Generally, the increase in the fatigue life by ion implantation is attributed to the suppression or reduction of the slip band formation at the surface of the fatigued specimen.

It is now generally established that the fatigue failure

of single crystals and polycrystals of pure metals and alloys follow a general pattern which can be summarised as: plastic strain localization in slip bands, followed by slip band emergence at the free surface, causing surface damage accumulation, and finally initiating fatigue crack, which propagates to cause catastrophic failure. With ion beam surface modification, a hard surface layer can be formed which can resist and delay the emergence of slip bands through the surface and thereby increasing the fatigue life.

There has been considerable research work in recent years on ion-implantation to improve the fatigue performance of various materials. Studies have been done on various model systems e.g, single crystals and polycrystals of pure metals as well as other engineering alloys. However, so far there has not been any study to characterise the effects of ion beam surface modifications on the fatigue behavior of dispersion strengthened alloys. These alloys have unique cyclic plasticity behavior which are very different than that of pure metals and alloys. In these alloys, the presence of fine dispersions of hard particles in the matrix causes extensive cross-slip in their vicinity. Consequently, long range slip localization is prevented, resulting in a more homogeneous slip distribution [Leverant,1968]. The present study is intended to investigate how surface modification by ion implantation can affect the fatigue behavior of such materials.

For the present work, thoria-dispersed nickel (DS-Nickel) has been chosen as the base material and aluminum ion implantation has been used to modify its surface. The choice of DS-Nickel as the base material has been motivated by the fact that recently extensive work has been done on the effect of aluminum ion implantation on the fatigue behavior of pure Nickel [Ahmed,1985; Grummon,1987]. The cyclic plasticity behavior of pure nickel with aluminum ion implanted surface layer has been well characterised. Subjecting DS-nickel to similar experimental conditions, it would be possible to know how this matrix, having a different cyclic plasticity behavior, interacts with the ion-implanted layer and how that affects the fatigue behavior of the material. Furthermore, DS-Nickel is a representative of a whole family of dispersion strengthened alloys and thus the knowledge gained from the study of DS-Nickel can also be applied to other materials belonging to this important class of materials.

CHAPTER II

REVIEW OF THE LITERATURE

Over the past few decades, considerable research work has been done on cyclic deformation of fcc materials. While most of these studies were done on model systems including pure metals and alloys, there has been some studies on the monotonic as well as cyclic deformation behavior of dispersion strengthened alloys. In this section, some of those studies will be reviewed which are relevant to the present study. Also, there has been substantial research in the application of ion-beam surface modification to improve the cyclic deformation behavior of various materials. Later, in this section, some of those works will be reviewed.

Cyclic Stress-Strain Response of FCC Materials

When a material is subjected to cyclic loading above the "fatigue limit", it fails after a finite number of load cycles. This type of failure mode is known as fatigue failure. Ewing and Humphrey (1902) first obtained clear microscopic evidence of slip on the surface of the fatigued specimens and could relate the mechanism of fatigue to plastic deformation of the material. Today, it is fairly well established that the stress amplitudes that cause fatigue failure, although for most cases too small to cause

any "macro-yielding", are large enough to cause cyclic "micro-plastic" strains of the order of 10^{-4} to 10^{-5}. These small strains accumulated over a large number of cycles can add up to a very high localized accumulated strain and can thus initiate fatigue cracks, which then propagate to cause failure.

The relation between the cyclic plastic strain amplitude ϵ_{pl} and the fatigue life N_f was first formulated by Coffin and Manson (1954) by the Coffin-Manson law which states that

$$N_f \cdot \epsilon_{pl} = k \text{ (constant)} \quad \ldots\ldots (1)$$

For most pure fcc metals and alloys, when cycled within a critical range of plastic strain of the order of 10^{-4} to 10^{-3}, slip becomes localized into "Persistent Slip Bands" or PSBs. PSBs correspond to lamellae of high local glide activity. They usually lie parallel to the primary glide plane and can extend deep into the bulk (Helgeland, Roberts et al,1965) and have typical thickness of about 1 μ in pure fcc metals (Mughrabi,1978). Broom and Ham (1959) and Finney and Laird (1975) showed that at intermediate cyclic strain amplitudes, slip is essentially confined to the PSBs. Slip within the PSB is to some extent irreversible which means that the slip during the forward and reverse cycle do not necessarily take place in the same atomic planes (Watt, Embury & Ham 1968, Finney & Laird 1975). This irreversible nature of the slip within the PSBs leads to the formation of

slip-steps at the surface and the slip traces develop a marked relief (notch-peak geometry) which serves as the preferential site for fatigue crack nucleation.

The formation of persistent slip bands is most likely to occur where a single slip system is active and PSBs form easily in single crystals. However PSBs have been observed in polycrystals also, but only in grains that are oriented for single-slip and at low strain amplitudes where single slip is favoured over multiple slip. From the viewpoint of fatigue crack initiation, the net extrusion of the PSB as a whole is identified as a type I stress raiser, while the notch-peak topography of the PSB surface as type II stress raiser. The shear cracks are likely to initiate early at the PSB-matrix interface due to type I stress raisers, which are known to form early. At a later stage, they are likely to initiate at the protruding surface of the PSB, where the type II stress raisers cause severe stress concentration (Mughrabi & Wang,1982).

Monotonic Deformation of Dispersion-Strengthened Materials

Extensive research work had been done on the monotonic tensile behavior of dispersion-strengthened and precipitation-strengthened alloys. Ebeling and Ashby (1966), Jones and Kelly (1968-69) and Hirsch and Humphreys (1970) had done extensive work on the tensile behaviour of internally-oxidised copper alloys. Most of this work have

been directed to explain the yielding of dispersion-strengthened alloys in terms of "Orowan mechanism". According to Orowan's mechanism, the yield stress of the alloy is inversely proportional to the particle spacing by the following relation (Orowan, 1948),

$$\sigma_y = \sigma_m + 2T / bD \qquad \ldots\ldots (2)$$

where σ_y is the alloy yield stress, σ_m is the matrix yield stress in shear, T is the dislocation line tension, b is the Burger's vector and D is the particle spacing. The particle spacing D is defined as ($1 / \sqrt{N_s}$) where N_s is the number of particles intersecting unit area of the glide plane. So, for a given volume percent of the dispersoid, the finer the dispersion, the higher is the yield stress. However, there is a critical size for the dispersoids, below which the shearing or fracture of the dispersoids is favoured over gross yielding of the matrix. In fact, Orowan mechanism suggests that there is a critical size for the particles, below which the particles are sheared off and above which they are bypassed by the dislocations. Kupcis, Ramaswami and Woo (1973), also working on internally oxidised copper alloys, showed that when non-coherent alumina particles were greater than 40 nm in size, the crystal yielded at a stress suggested by Orowan mechanism, indicating the by-passing of the particles by the dislocations. However, when the particles were less than 15 nm in size, the material showed much lower yield strength

than required by Orowan mechanism, suggesting the shearing of the coherent particles by dislocations.

Ansell and Lenel (1960) proposed that the yielding of dispersion strengthened alloy occurs when the shear stress on the particle becomes equal to either yield or fracture stress of the particle. According to this model, the yield stress of the alloy is given by,

$$\sigma_y = \sqrt{} (\mu b \mu^* / 2\alpha C) \quad ..... \quad (3)$$

where μ and μ^* are the shear moduli of the matrix and the particles respectively, b is the Burger's vector, α is the particle spacing and C is a constant. When the shear stress due to the pile-up of dislocation loops around the particles becomes high enough to deform or fracture the particles, gross yielding occurs, relieving the back stress on the dislocation sources.

The early model of yielding of a dispersion strengthened alloy as proposed by Orowan (1948) was modified by Friedel (1964) and Kelly and Nicholson (1964). According to them, The critical stress required to push a dislocation between two non-deforming particles of distance D was given by the modified form,

$$\sigma = A (Gb / 2\pi D) \ln (D / b) \quad ..... \quad (4)$$

where, $A = [\ 1 + (\alpha\ /\ 1-\alpha)\ \mathrm{Sin}^2\theta\ ]$

Here σ is the critical shear stress, G is the matrix shear modulus, b is the Burger's vector, α is the Poisson's ratio and θ is the angle between the Burger's vector and the dislocation line with no stress applied. (So, θ = 0 for a screw dislocation; and θ = 90 for an edge dislocation).

Ashby (1966) pointed out some of the discrepancies of the above treatment by Kelly & Nicholson. In his analysis, Ashby took under consideration two factors which were neglected by earlier workers e.g, a) the Orowan stress can be reduced by the mutual interaction of two bowed-out segments and b) the dislocation may dissociate into partials and thereby reducing its line tension and energy. The result of his analysis was a further modification of equation (4).

The fracture mechanisms of internally oxidised Copper alloys containing a uniform dispersion of very fine (50-70 nm) oxide particles, was studied by Palmer and Smith (1966). They investigated the fracture of single-crystals and polycrystals under monotonic tensile deformation and observed that the failure was initiated at the particle-matrix interface, due to void nucleation on the oxide particles. Fracture occurs by void growth and coalescence, with extensive coalescence being confined to the plane of fracture. They also observed that as far as void nucleation is concerned, the oxide particles in the grain boundaries

behave in much the same way as those in the grain interior.

The formation of dislocation substructures in TD-Nickel under monotonic tensile deformation was investigated by Heimendahl and Thomas (1964). Upon observing the microstructure of plastically deformed specimens, they reported that the dislocations are pinned and tangled around the thoria particles. The dislocation loops around the particles were often elongated, indicating the avoidance of the particle by cross slip. Dislocation loops were often prismatic and not concentric as proposed by Fisher et. al. (1953). After large deformation (≈ 10%), the dislocations tended to form a cellular structure whose size was governed by the spacing of the thoria particles. The dislocation cell structure in TD-Nickel was not as well developed as in pure nickel and the size of the cells in TD-nickel was about five times smaller. However, after very high deformation (≈ 90%), the dislocation cell structure in TD-Nickel was well developed.

Inman, Zwilsky and Boone (1964) investigated the microstructural features of cold-rolled and recrystallised TD-Nickel to gain insight on the strengthening effect of the fine second phase particles. The microstructure of heavily deformed TD-Nickel consists of elongated cells or fibres and it shows a strong texture of (110)[001]. The recrystallisation of TD-Nickel occurs at about the same temperature range as that of pure nickel. The recrystallised

TD-Nickel shows a primary texture of (100)[001] with a secondary texture of (110)[112]. The recrystallised TD-Nickel showed a large number of annealing twins. The mean particle size in TD-Nickel was about 50 nm.

Presence of a large number of narrow annealing twins was also reported by Heimendahl and Thomas, who investigated the microstructural feature of annealed TD-Nickel. The twin boundaries were very irregular and thus indicated that the thoria particles resist twin growth. Twin boundaries act as barriers to dislocation motion and thus contribute to its strengthening mechanism. Also, the thoria particles were never seen to be intersected or fractured by the dislocations. The yield stress of TD-Nickel appeared to be much higher than that predicted, on the basis of particle size and spacing, by the extended Orowan equation,

$$\sigma_y = \sigma_s + (Gb\phi / 4\pi) \ln [(d-2r) / 2b] [2 / (d-2r)] \quad \ldots\ldots (5)$$

where G is the shear modulus of matrix, b is the Burger's vector, r is the mean particle radius, d is mean planar interparticle spacing, σ_s is the yield stress of matrix, $\phi = 0.5\{ 1 + 1 /(1-\alpha)\}$, and α is Poisson's ratio.

The Orowan equation however is only applicable to single crystals. Polycrystals show much higher yield stress and this increase in yield stress is due to the additional contribution from grain boundaries, twin boundaries and

texture (Heimendahl and Thomas, 1964).

The various works discussed so far, dealt with the monotonic deformation of dispersion strengthened alloys. The mechanical behavior of these alloys under monotonic deformation has been well characterised both in the macro and micro-level. However, for the present study, it is more important to review the studies that dealt with the cyclic deformation and fatigue behavior of dispersion strengthened alloys.

Fatigue Behavior of Dispersion-Strengthened Materials

The cyclic deformation behavior of dispersion strengthened alloys differs significantly from that of pure metals and alloys. The hard particles in the matrix are known to cause the plastic strain homogenisation and thereby resisting persistent slip band formation. As a result, fatigue crack initiation is much more difficult in these alloys. Several studies has been done on the cyclic deformation behavior of dispersion strengthened alloys and some of the relevant ones are reviewed here.

Wells and Sullivan (1964) characterised the low-cycle fatigue behavior of a Nickel-base superalloy (Udimet 700) whose microstructure contains random distribution of hard second-phase particles. The initial cyclic hardening of this

material is followed by cyclic softening which is due to the fracture of the precipitates. Intense slip band formation is observed and slip-band cracking along with twin-boundary cracking are believed to be the dominant mode of crack initiation.

Abel and Ham (1966) studied the cyclic strain behaviour of precipitation-strengthened aluminum alloys and pointed out that the Bauschinger effect was extremely high in those systems when the precipitates were not coherent. They explained it in terms of internal stresses being built up at the particles during forward flow. They also reported very fast cyclic hardening, sometimes followed by softening, when the precipitates were not coherent. Occasional cracking at the particles were also reported. The rapid strain hardening behavior of dispersion strengthened alloys are generally attributed to rapid multiplication of dislocations due to multiple slip systems. This effect is further aided by the back stresses developed by the dislocation loops at the particles.

Leverant (1967) investigated the fatigue behaviour of thoria-dispersed nickel to find out whether the fine dispersion of hard particles can induce irreversibility in the cyclic plasticity behaviour of a wavy-slip material by stabilizing the initial microstructure. Based on the results obtained, he concluded that the presence of these fine, hard particles did not affect the reversible cyclic plasticity

behaviour of a "wavy-slip" material at room temperature.

The presence of a fine dispersion of hard second-phase particles in an otherwise pure matrix can significantly alter the fatigue behaviour of fcc materials. The most significant change may take place in the extent of cyclic plastic strain localization during fatigue. Leverant and Sullivan (1968) studied the effect of a fine dispersion of Thoria particles on the fatigue behaviour of pure nickel. They observed that the extent of surface slip was greatly reduced by the presence of thoria particles and the slip was more wavy and heterogeneous as compared to that in pure nickel.

The reduction in the extent of surface slip and the development of much finer slip can be attributed to the fact that the fine, hard particles, uniformly dispersed over the matrix, offer resistance to slip and cause extensive cross-slip in their vicinity. As a result, the localization of slip over large distances is not favoured, thus giving rise to a fairly homogeneous distribution of slip throughout the matrix. Furthermore, since crack initiation is greatly influenced by the extent of strain localization, it follows that fatigue crack initiation will be more difficult due to the presence of these fine particles (Leverant & Sullivan, 1968).

Another important feature due to the presence of these

particles is the effect on the dislocation substructure at saturation. Due to extensive cross-slip in the vicinity of the particles, dislocation cell-walls are formed, with the particles being included in the cell walls. The size of these cells is independent of the plastic strain range and is controlled by the size and distribution of the second-phase particles (Leverant and Sullivan, 1968). The formation of this dislocation substructure and the dependence of their size on the distribution of second-phase particles is also evident in the monotonic deformation behavior of Thoria Dispersed (TD) Nickel (Heimendahl and Thomas, 1964) and other dispersion strengthened alloys (Kimura,1965; Ashby,1964).

Further work by Mori and Mura (1976) on the slip morphology of dispersion strengthened materials showed that although in general the plastic deformation in these alloys is homogeneous, heterogeneous plastic deformation sometimes does occur in a certain range of plastic strain if the alloy contains softening particles, as in quench-hardened aluminum or neutron irradiated copper.

The cyclic deformation behavior of a precipitation hardened Al-Ag alloy was investigated by Laird et. al. (1978). They observed that the alloys containing Guinier-Preston (GP) zones did not cyclically soften. This supports the "disordering" mechanism of cyclic softening of alloys containing ordered precipitates, since GP zones are

inherently disordered. They also observed the formation of cyclic strain induced stable precipitates.

Wilhelm (1980), investigating the cyclic plasticity behaviour of age-hardened copper and aluminum alloys, reported that below a threshold plastic strain range of the order of 0.0001 - 0.0002, the alloys cyclically hardened to a saturation stress. No PSBs are formed and the coherent precipitates are not destroyed by the gliding dislocations. However, when cycled at higher plastic strain, PSBs do form at a critical stress and the material shows cyclic softening. The cyclic softening is attributed to the destruction of shearable precipitates within the PSBs by the gliding dislocations.

Vogel, Wilhelm and Gerold (1981) investigated the development of the microstructure during the cyclic deformation of peak aged Al-Zn-Mg single crystals. When cycled under constant plastic strain ($\approx 10^{-3}$), slip bands are formed initially which grow in volume and also in dislocation density. At a critical dislocation density, the slip bands collapse into a secondary slip band structure which permits higher dislocation density. The precipitates are sheared and destroyed within these bands and finally narrow PSBs are formed which are devoid of any particles. The material within the PSB remains in a supersaturated solid solution state.

Steiner and Gerold (1986) investigated the fatigue behavior of single crystals of Cu-2at.%Co alloy. The general sequence was found to be Cyclic hardening, the formation of PSBs and cyclic softening. The cyclic softening had been attributed to the dissolution of the precipitates within the PSBs.

To summarize, it has been observed that the presence of fine, hard particles or precipitates in the matrix, substantially reduces the extent of plastic strain localization in PSBs. This results in a more homogeneous distribution of plastic strain over the matrix, thereby hindering the fatigue crack initiation. The stability of the particles or the precipitates under cyclic deformation are critical for the improved fatigue performance of dispersion-strengthened alloys and precipitation-hardened alloys as well. If the second phase particles or precipitates are fractured or dissolved in the matrix during cyclic deformation, the alloy shows a cyclic softening with the subsequent formation of PSBs and the overall fatigue performance is adversely affected.

The Effect of Surface Modification on Mechanical Properties

Substantial amount of research work has been carried out in recent years to characterise the effects of various surface modification techniques on the mechanical behaviour of materials. It has been shown by various researchers that the mechanical deformation behavior of the materials can be influenced by modifying the state of the surface. This is associated with the structural changes in the crystal lattice in the surface and sub-surface regions and the corresponding dislocation dynamics in these regions. Some fundamental studies in this aspect are reviewed here.

Initial work by Koehler (1941) showed that an image force is active on a screw dislocation present near an interface between two materials having different elastic moduli. If the dislocation lies in the material of higher elastic modulus, it is attracted towards the interface under the image force, whereas the dislocation is repelled if it is in the material of lower elastic modulus. Head (1953), working with a surface of higher elastic modulus than the bulk, concluded that for a thin, hard surface layer, the screw dislocations will assume an equilibrium position near the interface where the image force acting on the dislocation is at its minimum. Further work on the image force on the screw as well as edge dislocations were carried out by Chou (1966) & Conners (1967), for a more generalized combination of the

surface and the bulk elastic moduli as well as the surface layer thickness. They showed that for a particular combination of the surface layer and the bulk material, the thickness of the surface layer is critically important, because it determines the magnitude and the direction of the image forces in the surface layer and the bulk. Greenfield (1973) showed that the principal hardening mechanism for a thin diffused surface layer is by means of an accomodation dislocation network. He also concluded that this accomodation dislocation network is greatly influenced by the nature of the image forces in the surface layer and in the bulk.

DeJonghe and Greenfield (1969) reported a considerable increase in the critical resolved shear stress (CRSS) of copper single crystal having platinum diffused surface layers. The surface hardening was attributed to an accomodation network of dislocations. A later work by Greenfield (1973) was reported to have increased the CRSS of copper single crystal by diffusing surface layer of platinum, gold, silver and nickel as well. Again the surface hardening was attributed to the accomodation dislocation network.

A detailed study was undertaken by Greenfield and Purohit (1980) to classify the effects of surface modification into some broad categories. They worked with both discrete and diffused surface layers and analysed the results in terms of

image forces, dislocation initiation and accomodation networks. The main variables of the experiments were the elastic modulii, yield stress and yield strain of both the surface and the bulk for various systems. One particular combination of interest is when the surface has lower elastic modulus but higher yield stress than the bulk. In this case, during cyclic loading, the stress at the surface will initially be lower than the bulk and also the yielding of the surface is less likely. In a situation like this, it is possible, for a specified range of applied stress, that the surface layer cycles elastically while the bulk sustains cyclic micro-plastic strain. Even though the bulk material accumulates plastic strain, the surface layer does not incur any damage. However, when bulk plastic strain accumulates to a critical value, the surface layer will rupture, leading to permanent surface damage. This process would require considerable period of time and would be manifest in an improvement of fatigue life.

In a recent study by Meyers and Grummon (1988), finite element method has been used to model the micromechanics of the interaction between the ion implanted surface layer and the underlying persistent slip band. The surface film in Al^{+} ion beam modified nickel substrate was found to rupture as a result of high stress concentration at the film due to the slip activities in the underlying subsurface slip band. However, the rupture of the surface film does not occur until a considerable amount of plastic strain is accumulated

and this results in a delay in the fatigue crack initiation of ion beam modified specimens, causing higher fatigue life.

In recent years, ion-implantation has emerged to be a very versatile process for surface modification. Considerable amount of research work has been done and is still being conducted on the beneficial effect of ion implantation to improve the mechanical, chemical and environmental properties of a wide range of materials. We will discuss some of the salient features of ion implantation process and the potential use of this process to improve the fatigue properties of various materials.

Ion-Implantation Process and Characteristics

Ion-Implantation is a process where ions of an atomic species to be implanted are generated and accelerated through very high voltages and are made to impinge onto the target. The process must be carried out in vacuum ($\approx 10^{-6}$ torr.), otherwise the ion beam will be scattered and absorbed over a short distance and also the surface chemistry of the target cannot be controlled.

The main parameters that characterise the ion implantation process are:

a) the ion species to be implanted;

b) the target species ;

c) kinetic energy of the ion beam;

d) the number of ions per unit area of target (fluence);

e) the beam current ;

f) the total implantation time ;

g) the target temperature during ion implantation.

Some of the salient features of ion-implantation process that make it especially attractive as a tool for tailor-made surface engineering are as follows ,

1) The process is extremely versatile. Almost any atomic species can be implanted into a broad class of materials including metals, ceramics and polymers.

2) The process can be carried out at room temperature without causing any major changes in the bulk properties.

3) Since the process is not entirely governed by the thermodynamic criteria, many non-equilibrium phases can be produced. Also solid solutions beyond the thermodynamic solubility limit can be created by this process.

However there are some disadvantages to this process of which the most important ones are the line-of-sight limitation and high cost.

To gain an insight into the kinetics of the ion implantation process, let us look at the physical processes that take place during ion implantation. As the energised ion impinges onto the target, it is rapidly slowed down as it continually loses its kinetic energy due to interactions with the electrons of the target atoms. Also it transmits quanta of energy whenever it collides with the target nuclei

and as a result of that, a number of target atoms are knocked off their lattice sites in a cascading manner. Due to a large number of incident ions, random movement of ions occur in a cascading manner, leading to random mixing of the ions. In fact, ion-beam mixing is one of the commonly used method for surface modification. This mixing process can be compared to the thermal diffusion process, however it does not have any temperature dependence, instead the extent of mixing is dependent on the implanted species, substrate and beam energy. The energy transfer process between the incident ion and the target atoms also dictates the deposited ion concentration profile. Usually the implanted species assume a gaussian distribution near the surface of the target material. The depth corresponding to the peak of the Gaussian distribution is called the "Range". The range is again a function of the implanted species and beam energy. Due to the surface expansion effect as well as sputtering of target atoms, the resulting concentration profile deviates from an ideal gaussian distribution and in fact, the experimental data fit more closely to "Pearson IV" distribution. Nowadays, computer codes (e.g, "Profile" from Implant Sciences, Danvers, MA) are available to compute the concentration profile of the implanted ions given the process parameters.

Effect of Ion Implantation on Fatigue Behavior

As mentioned earlier in this section, there is growing

evidence that the mechanical deformation behavior of the material can be influenced by altering the surface layer. It is now generally established that fatigue cracks usually originate and propagate from the free surface of the specimen. Thus the surface condition plays a major role in the fatigue performance of the specimen. If proper surface modification is employed, it is possible to manipulate the deformation behavior in the surface as well as sub-surface regions in such a way so as to prohibit fatigue crack initiation at the free surface. Since ion implantation has emerged in recent times to be a very flexible tool for surface modification, considerable research has been carried out to modify the surface of various materials using ion implantation, in order to improve their fatigue performance.

One of the earlier studies in this area was undertaken by Kujore, Chakraborty, Starke and Legg (1980), who studied the effect of aluminum ion implantation on the fatigue crack initiation of pure polycrystalline copper. The fatigue life of copper was found to increase, after Al^+ ion implantation, by about 35% in high cycle fatigue under stress control. Upon closer examination of the surface topography, they observed that the extensive formation of coarse PSBs in unimplanted copper is replaced by a less severe formation of finer PSBs in implanted specimens. They argued that the increse in fatigue life was due to the relatively homogeneous slip and finer slip bands in the implanted species. It was postulated that the introduction of aluminum

in copper resulted in lower stacking-fault energy of the surface layer and that caused a decrease in the extent of cross slip, thus promoting slip reversibility. Also, since Al^+ ions are larger than Cu^+ ions, a compressive residual stress pattern may have been generated on the surface, which would resist the formation of surface crack and thus help to increase the fatigue life.

Similar work was carried out by Sleeswyk, Kok and Boom (1980) to investigate the effect of C^+ ion implantation on the low-cycle fatigue life of copper, nickel and stainless steel polycrystals. The specimen temperature during ion-implantation rose to 100 °C. On Ion Implantation, the fatigue life of nickel was increased by about 10%, but surprisingly the fatigue life of copper and stainless steel was shortened by about 20%. This was consistent with the observation that the slip lines in implanted copper and stainless steel were much coarser than in unimplanted species. Although the authors could not give any satisfactory explanation of this rather unusual decrease in fatigue life of copper and stainless steel, they suspected that a high concentration of dislocations underneath the surface layer might cause micro-cracking parallel to the surface. Nickel, on the other hand showed an increase in fatigue life, which was associated with the formation of finer slip bands and lower stress concentration.

Bakhru et. al. (1981) studied the effect of Ne^+ and N^+ ion

implantation on bending fatigue performance of polycrystalline copper and austenitic stainless steel respectively. While Ne^+ implanted copper showed a significant increase in fatigue life, no such improvement was evident in N^+ implanted stainless steel. The surface of the unimplanted stainless steel showed profuse slip band formation, but after ion implantation, it showed fewer but more sharply defined slip bands. One significant observation was the presence of kinks in the slip bands, which indicated the tendency of cross-slip. The occurence of cross-slip in stainless steel is usually rare, because of its relatively low stacking fault energy. The authors speculated that the presence of large concentration of N atoms in implanted layer, which acts as obstacles to dislocation glide, necessitates higher shear stress in the slip bands, which may then cause cross-slip. According to the authors, the beneficial effects of lattice hardening and compressive surface stresses due to ion implantation were offset by the detrimental effects of radiation damage and occurrence of cross-slip, resulting in no significant improvement in fatigue life of stainless steel. Copper, on the other hand, after implantation, showed almost no slip bands on the surface and thus explains the remarkable improvement in fatigue life.

Vardiman and Kant (1981) investigated the effect of C^+ and N^+ ion implantation on the fatigue life of Ti-6Al-4V alloy. They observed a 10% and 20% increase in the endurance

limit by N^+ and C^+ implantation respectively. From the fractographic analysis, it was found that for specimens with a lifetime less than 10^5 cycles, the fatigue crack was initiated at the surface. However, for specimens with a lifetime greater than 10^5 cycles, the crack showed a subsurface origin. The subsurface origins occured at a depth of 25-150 μ. The authors did not give any satisfactory explanation of the observed increase in fatigue life by ion implantation. Also, the sub-surface initiation of the fatigue crack was not fully explained.

Another investigation was done by Mendez, Violan and Villain (1982), to study the fatigue behavior of copper polycrystals with ion implantation of various elements e.g, Cu, Al, O and N ions. The most significant observation was that the N and O ion implantation lead to severe inhibition of surface slip bands, while this effect was not so severe with Cu and Al ion implantation. Based on their findings and some earlier reports, the authors generalised that the implantation of gaseous elements is almost always associated with the inhibition of slip bands. They also stated that the implantation of gaseous elements often lead to the formation of gas bubbles in the implanted layers, which act as dislocation sinks, thus preventing the egress of dislocations on the surface.

Extensive work was done by Jata and Starke (1983) to characterize the effects of ion implantation on the fatigue

performance of a wide range of materials including copper, aluminum, titanium and steel. They identified the formation of several metastable and stable phases in each of the substrates during implantation of various species. They reported fatigue life improvement in Cu implanted with Al^+, Cr^+ and B^+ and also in Ti-24V alloy implanted with Al^+. This improvement in fatigue life was associated with much finer and homogeneous slip at the surface in the implanted species. In general, transgranular cracks were observed in unimplanted species, while implanted species showed intergranular cracks initiating at the interface of persistent slip bands (PSB) and grain boundaries. The result of fatigue tests on self-implanted copper did not show any appreciable improvement, suggesting that the lattice damage caused by ion implantation, although quite severe at times, does not significantly contribute to fatigue life improvement. However, ion implantation did not always produce positive results. In fact, α/β Ti implanted with Al^+ and 4140 steel implanted with N actually showed a decrease in life in strain-controlled fatigue tests. However, both of these materials showed considerable improvement in life under stress-controlled fatigue tests. Also they pointed out that a residual compressive stress may be present at the surface when implanted with larger atoms. To utilize this compressive state of stress at the surface, one has to be careful not to overload the specimen, which would destroy the beneficial effect of the residual compressive stress. It must be noted, however that the

beneficial effect of a residual compressive stress at the surface cannot be easily isolated from the effect of metastable and stable phase formation during ion implantation.

Hohmuth, Richter, Rauschenbach and Blochwitz (1985) studied the effect of B^+ and N^+ ion implantation on fatigue of polycrystalline nickel. They found that the extent of surface slip bands were much lower in the implanted species. With increasing implantation dose, slip band density decreased, however the fatigue lifetime is maximum at an optimum implantation dose of 5×10^{17} ions $/cm^2$. This is probably because at very high dose, the complete prevention of PSB formation may lead to very high stress incompatibility between the grains, leading to grain boundary cracking. Another interesting point to note was the shift of the composition profile towards the surface after fatigue. The authors suggest that the cyclic deformation causes boron and nitrogen atoms to diffuse to the surface.

It has long been known that ion implantation can lead to metastable phase formation in near-surface region which plays important role in modifying the surface sensitive properties of the substrate. A very comprehensive study was undertaken by Follstaedt (1985) to characterise different metastable phases formed in various material systems. Of particular interest to us is the fcc -> hcp transformation of pure Ni subject to neutron irradiation or implantation

with Ar, He, P, Sb or even Ni. It is theorised that the stress accompanying ion implantation is mainly responsible for this phase transformation. Of even more interest is the formation of amorphous phases during metalloid ion implantation in metals. Rauschenbach et al. (1982-83) had already applied Hagg's embedment criterion (Hagg, 1931) to predict the formation of amorphous or crystalline phase in a particular material-implant system. According to the Hagg's rule, if the ratio (R) of the metalloid atom size to that of the metal atom is greater than 0.59, amorphous phases appear while $R < 0.59$ ensures crystalline phase formation. An interesting model system which has been fairly well characterised and which is of our interest too, is the Ni-Al system. For the Al-Ni^+ system, an amorphous phase nucleates in fcc Al and grows until a single amorphous phase is found at 25 at.% Ni. At even higher Ni content, crystalline AlNi phase forms within a matrix of the amorphous phase. For Ni-Al^+ system, we start with fcc Ni and go through an intermediate phase Ni_xAl, having 25-33 at.% Al and finally get similar phases i.e, the amorphous phase (25 at% Ni) and AlNi at higher Al content. It is interesting to note that neither Al_3Ni and Al_3Ni_2, which are the equilibrium phases, are found in any of these experiments.

Another contemporary study in this area was done by Ahmed and Potter (1985) who studied the microscopic processes accompanying Al ion implantation in Nickel. For specimens implanted to a fluence of 6×10^{17} ions/cm^2, the electron

diffraction pattern indicated the formation of the fcc (γ) solid solution and the solubility limit of aluminum in nickel was increased to about 30 at.% as compared to 10 at% at equilibrium. The γ' (Ni_3Al) phase does not form during implantation, instead an hcp phase is observed. Above 35 at% Al, this hcp phase is replaced by the ordered β'-NiAl phase. At even higher Al content ($\approx$ 60 at%), an amorphous phase is observed along with the β' phase.

A very detailed study was done by Wang et. al. (1985) to characterise the surface of ion-implanted and fatigued metals by transmission microscopy. They mainly investigated the surface of 304 stainless steel and copper implanted with N or Ne and proposed a model to explain the surface damage mechanism in the implanted layer. According to their model, a large number of uniformly distributed lattice defects, usually Frank loops, are formed after implantation. These defects resist dislocation glide. However, once penetrated by the glide dislocations, these loops are annihilated. As a result, there is little or poor resistance to dislocation glide and eventually dislocation channels are formed. These dislocation channels are similar to the PSBs formed in unimplanted metals. Cyclic slip is concentrated in these channels and eventually cause surface extrusion/intrusion damage, leading to fatigue crack initiation.

Vardiman and Cox (1985) did another study to improve the fatigue life of a Ni-Cr alloy using C ion implantation. They

reported about 17% improvement in fatigue performance which was again attributed to the suppression of surface slip by ion implantation. Solid solution hardening and compressive stress at the surface were believed to be the main factors behind reduced surface slip. The slip band cracking in unimplanted material was replaced by, as expected, grain boundary cracking in the implanted material.

Another recent study was done by Mendez, Violan and Denanot (1987) who investigated the effect of nitrogen ion implantation on the fatigue behaviour of various fcc materials including copper, aluminum and stainless steel. There was no significant improvement in the fatigue life of 2017 aluminum alloy or 316L stainless steel after ion implantation, however significant improvement was reported for N-implanted pure copper. For 2017 aluminum alloy, the cracks were reportedly nucleated due to the cracking or debonding of the inclusions and thus quite obviously ion implantation has little effect on fatigue life. For 316L stainless steel, although N-implantation drastically reduced the extent of PSB formation, cyclic slip is so highly localised that the implanted layer is believed to be sheared and there was no improvement in fatigue life. In pure copper, however, the reduction in PSB formation due to N-implantation does result in 50% increase in fatigue life. Also, they reported no influence of ion-implantation on the cyclic hardening rate.

More recently, Grummon et. al. (1987) have characterised the surface morphologies of ion beam mixed surface layer in pure nickel and correlated them with the mechanical behaviour under cyclic loading. They evaporated alternate layers of Ni and Al on a pure Ni substrate and ballistically mixed them with a high-energy Kr^{+} beam. The surface modification resulted in a substantial decrease in the number and intensity of surface slip band features. The morphology of the Persistent Slip Bands (PSB) in the modified specimens were different than those in the unmodified specimens. The PSBs in the modified species mostly showed a single slip step as opposed to the typical notch-peak topography that was observed in the PSBs in the unmodied specimens. Subsurface plastic strain localization took place in the implanted species within the PSBs which extended upto the implanted layer. However, the implanted layer finally ruptured under the high local stress from the impinging PSBs, but only at much higher accumulated strain.

As an extension of the latter work, the present research was undertaken to study the effect of ion implantation on the fatigue behaviour of DS-Nickel, which has a very fine dispersion of inert thoria particles in an otherwise pure nickel matrix. There have been several studies done on the effect of ion-implantation on fatigue behaviour of pure nickel and these have been reviewed. The obvious question that follows is what are the effects of ion-implantation on the fatigue behaviour of a material which is chemically

similar to pure nickel, but behaves differently under cyclic plastic deformation. As we have seen earlier, the interaction between the implanted surface layer and the underlying cyclically deforming substrate is significant, as it can modify various mechanical properties, particularly the fatigue behaviour of the base material. Thus our choice of DS-Nickel as the substrate was motivated by the fact that it is chemically similar to pure nickel but has a very different cyclic plasticity behaviour. The choice of the implanted species i.e, Al^+, was guided by the fact that several studies have been done in the past to characterise the ion-implantation dynamics of Ni-Al^+ system and by employing similar ion implantation system, we can compare the behaviour of DS-Nickel with that of pure nickel. In the past, there have been very few studies on the fatigue behaviour of dispersion-strengthened alloys. So, the present research is carried out with the hope that it will provide us with some insight on ion implantation and its effect on this important class of materials.

CHAPTER III

EXPERIMENTAL PROCEDURES

The experimental procedures used in this study can be subdivided into three broad categories: specimen preparation, low-cycle fatigue testing, and post-fatigue surface characterisation. Low-cycle fatigue testing involved characterising cyclic hardening behavior, cyclic stress-strain behavior, and fatigue life. Each section will be described below in detail.

Material

DS-Nickel was supplied by Sherritt Gordon Mines Ltd., Fort Saskatchewan, Canada in 0.045 inch thick sheet in hot-rolled and pickled condition. This is a powder metallurgy product, manufactured through hot isostatic pressing (HIP), followed by a controlled thermo-mechanical heat treatment schedule. Its nominal chemical composition is 98% Nickel and 2% Thoria (ThO_2) with the thoria particles, 10-40 nm in size, uniformly dispersed in a nickel matrix. The wrought product has a characteristic microstructure comprising of lamallae oriented along rolling direction in {100}<001> cube texture. (fig. 1). The typical chemical analysis of DS-Nickel is given in table 1.

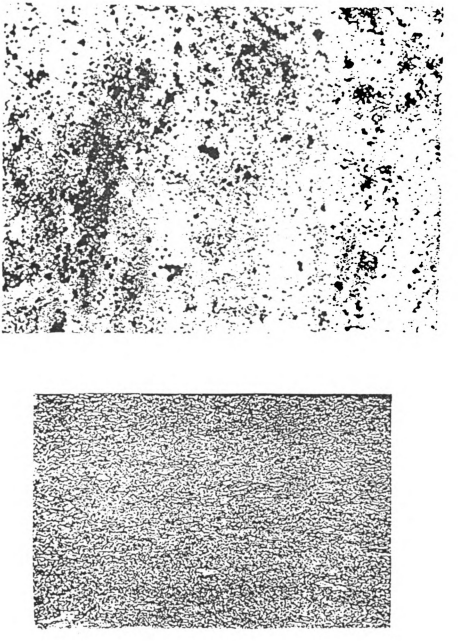

Fig. 1 : Transmission electron micrograph of DS-Nickel, (x 10,000)(top); Optical micrograph of DS-Nickel, (x 50)(bottom).
(Courtesy: Sherritt Gordon Mines Ltd.)

Table 1 : Chemical composition of DS-Nickel
[Courtesy : Sherritt Gordon Mines Ltd.]

Element	Weight (%)
ThO_2	2.1
C	0.005
S	0.001
Fe	0.020
Cr	0.003
Co	0.005
Ni	Balance

Specimen Design

The design of a proper specimen for fatigue testing of such a thin sheet proved to be a serious problem. There was no standard ASTM specimen design for such thin sheets. When designing a good fatigue specimen, proper attention must be paid to several critical factors, such as minimum stress concentration in the neck region and minimum tendency of buckling at the gauge section. For a thin sheet, there is an acute tendency toward buckling in compression and the most effective means of reducing this buckling tendency is to reduce the gauge length as much as possible. However the availability of a very small axial extensometer posed a lower limit on the gauge length at 6 mm. An optimum fillet was provided at the neck region to minimize stress concentration. This design was used to prepare the "Straight-edge specimens", which were used to characterise the cyclic hardening and cyclic stress-strain response under constant plastic strain (fig. 2).

The "Straight-edge specimens" required a finite straight gauge section so that an extensometer could be mounted to be used to measure and control the plastic strain during cyclic deformation. However the "Stright-gauge specimens" were not suitable for fatigue life determination experiments, because they were prone to buckling after large accumulated plastic

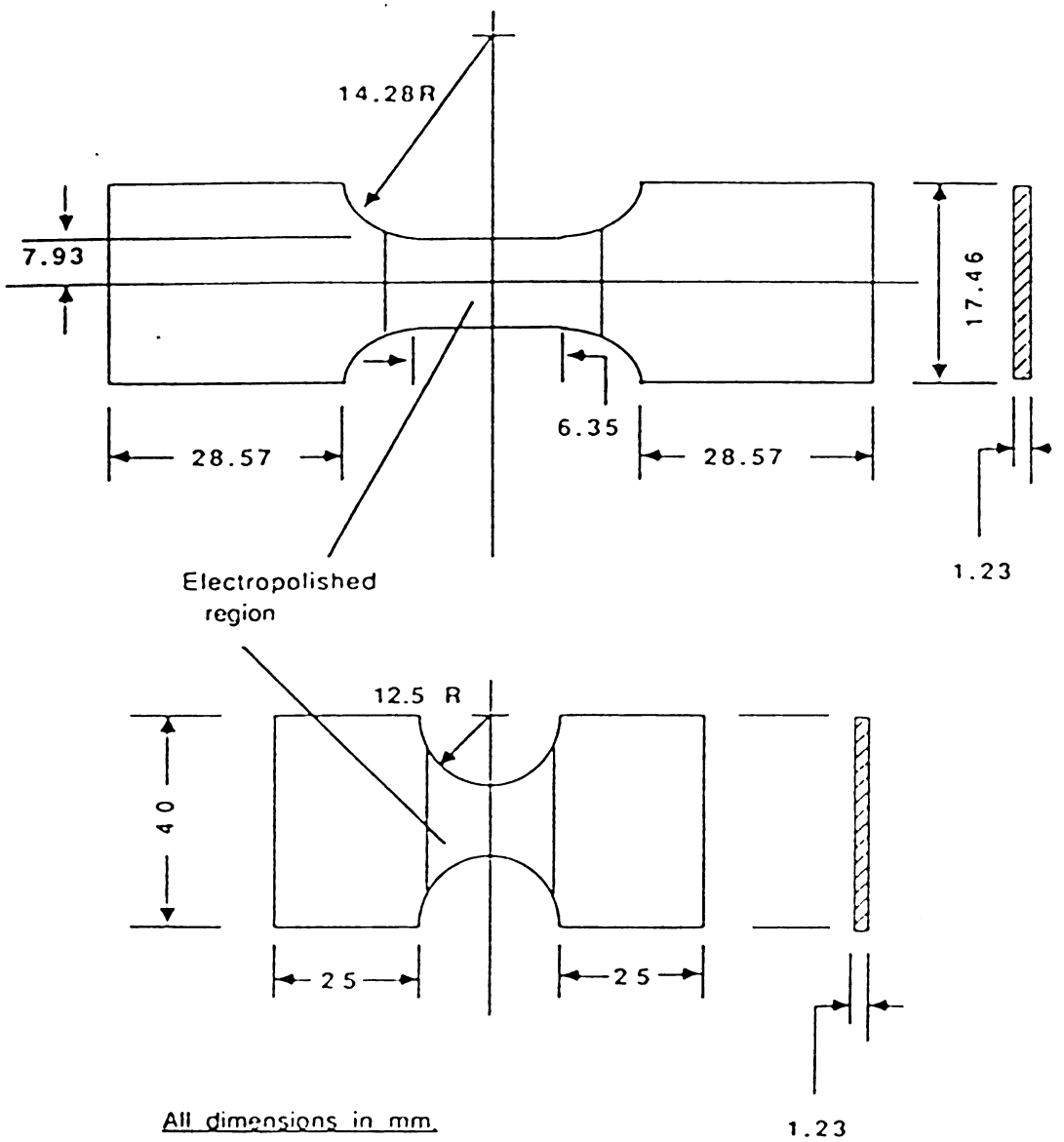

Fig. 2 : Specimen Designs for Fatigue Testing. Straight edge specimens (top) ; Hour-glass specimens (bottom).

strain. So a new specimen design with higher resistance to buckling was needed that could be used to determine the fatigue life of DS-Nickel.

A better choice for this purpose was the hourglass design, which essentially had no gauge length and was thus quite resistant to buckling. The straight edge specimens were used to establish a load increment schedule during cyclic hardening and cyclic stress-strain characterization. This loading schedule was used to subject the hourglass specimens to programmed cycling for fatigue life determination.

Machining and Surface Preparation

The machining of the specimens were done under close tolerance i.e, within 0.001 inch of the nominal dimensions. The straight-edge section specimens were machined in an NC milling machine, ensuring smooth edges with minimum undercut at the neck. The hour-glass specimens were punched out of the sheet, using a pneumatic press. Since DS-Nickel is mildly radioactive, special precautions were taken during machining to minimise chip formation and to ensure operator safety. After the initial machining, the edges were carefully smoothed and bevelled by fine filing. The machined specimens are then hand-polished with 600 grit abrasive paper followed by cloth-polishing with ultra-fine diamond paste to a mirror finish. The specimens were then rinsed and

cleaned in acetone and dried under air-jet.

The specimens were then dipped in lacquer to mask off the grip regions leaving only the gauge section and the neck region to be exposed to electro-polishing. The specimens were given two consecutive lacquer coatings with an intermediate air-drying for an hour. Specimens were left overnight after the final coating to thoroughly dry out. A small area of lacquer coating in one corner of the specimen was wiped clean with acetone to make electrical connection during electro-polishing.

Electro-Polishing

The electro-polishing was done at room temperature with an electrolyte made of 40% soln. of sulphuric acid in water. The electro-polishing was carried out at about 5 volts dc with a current density of 0.028-0.030 amp/mm^2, with mild stirring to ensure uniform polishing. The specimen was made the anode while an inert nickel sheet, bent to an annular shape, was used as cathode. The specimen was tightly secured to the jig so that it did not wobble during polishing. The polishing was completed in 50-60 seconds, resulting in a highly polished, smooth surface. The electro-polished specimens were then cleaned in water and the mask was fully dissolved in acetone. The specimens were finally rinsed and cleaned in acetone and methanol and dried under air-jet and stored in a dessicator prior to ion implantation.

Ion Implantation

The ion implantation was carried out at Michigan Ion Beam Laboratory using the 400 kV Varian Ion Implanter. Direct implantation of Al ions was carried out at 350 keV to a fluence of 5×10^{17} ions/cm^2. The specimen chamber is maintained under a very high vacuum ($\approx 1.5 \times 10^{-7}$ torr.). The specimens were ion-implanted in two batches with 5 specimens in each batch. They were clamped together in a special fixture to expose only the gauge area of both sides of the specimens to the ion beam. The beam was scanned over the target area to ensure uniform deposition. The total dose was monitored and controlled by a current integrator, which was preset to a calculated value corresponding to a definite thickness of the implanted layer. The current integrator calculation is given below :

$$D = N \cdot S / A \cdot e \quad \ldots\ldots (6)$$

where

D = dosage (ions/cm^2)

N = Current integrator count

S = Integrator scale

A = Aperture area

and e = electronic charge

During ion implantation, the specimens were allowed to heat up and the specimen temperature was measured every 30

minutes by means of a thermo-couple. The specimen temperature increased slowly during ion-implantation and reached a steady state value of 500 °C. Each batch of specimens took about 5 hours for ion implanting on each side. The processing parameters were maintained constant in both batches to ensure uniform processing. After ion implantation, the specimens were cooled down to room temperature under high vacuum to avoid surface oxidation. Finally, they were stored in a dessicator for fatigue testing.

Post-Radiation Surface Analysis

The ion-implanted specimens were observed under scanning electron microscope and phase contrast optical microscope to detect any surface damage that may have occured during ion implantation. The specimen surfaces were absolutely clean and smooth and did not show any sign of surface damage due to ion implantation. However in some specimens, the surface did show some very fine features which resulted from sputtering during ion implantation. The surface chemical composition was estimated using a special-purpose software ("Profile" from Implant Sciences, Danvers, MA). The Al^+ ion concentration near the surface approximately followed a gaussian distribution (fig. 3) with a projected range of 230 nm. This estimation is known to fit very closely to actual measurements.

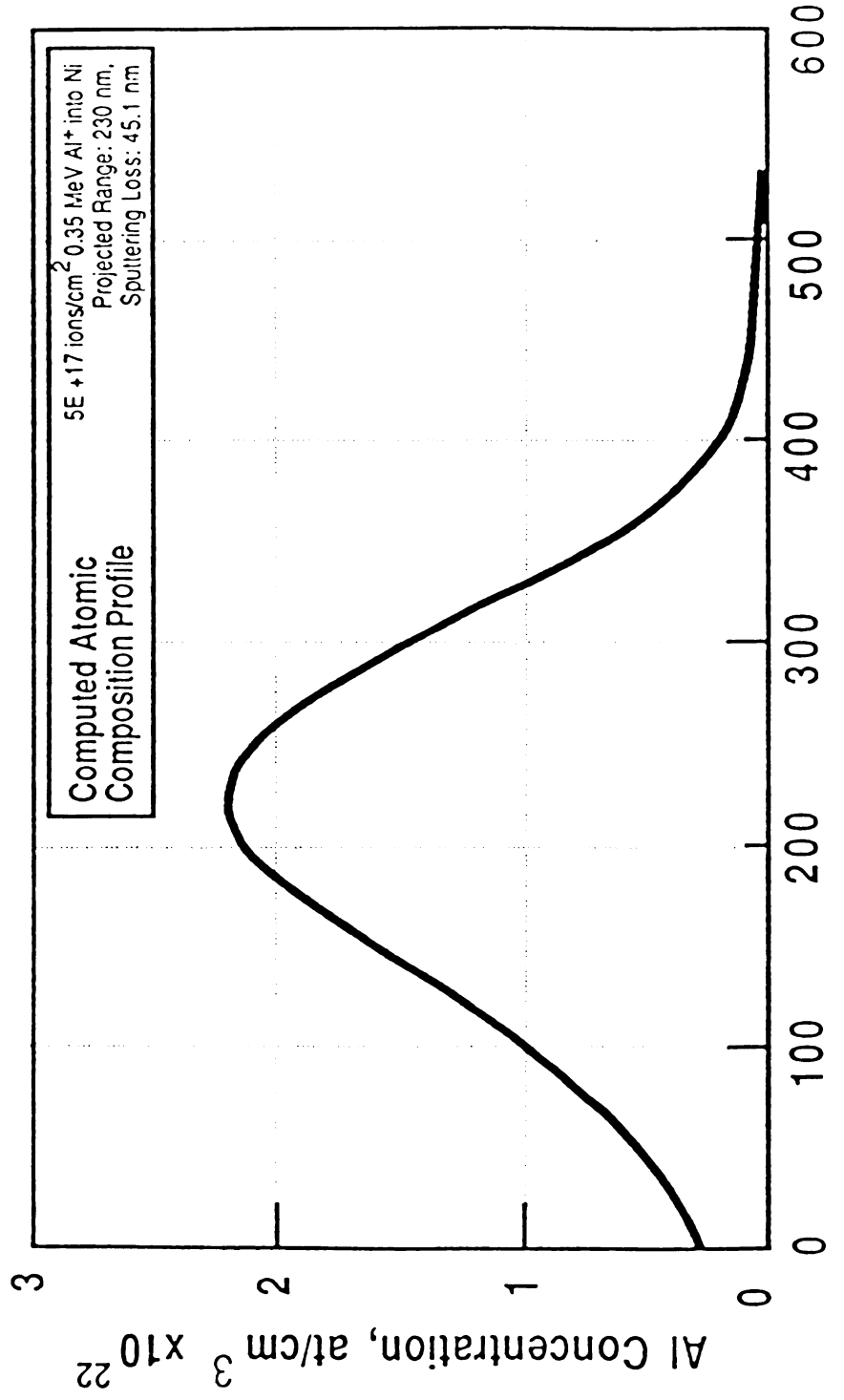

Fig. 3 : Surface Concentration Profile of Ion-Implanted Specimens

Low Cycle Fatigue Testing of DS-Nickel

Hardware

The low cycle fatigue testing of DS-Nickel was carried out with a closed-loop servohydraulic testing machine (MTS 880) equipped with a 20,000 pounds load cell and a 5.0 mm gauge length (MTS 632-29C-30) extensometer. The electronic noise level of the control circuitry was less than 5 millivolts in both the load and strain channel. For our thin sheet specimens, the proper alignment of the specimen within the hydraulic grips was extremely important and care was taken to minimise any misalignment. Also to ensure proper uniaxial stress state in the specimen, special care was taken to avoid any torsional loading of the specimen that might result from the rotational motion of the floating hydraulic ram. A special fixture was designed to this effect in the form of an aluminum bar fixed to the bottom hydraulic grip which would slide up and down along the side-posts of the machine and would thus prevent any torsional motion of the floating grip. To ensure proper gripping of the specimens in the hydraulic grips, small rectangular tabs, made of mild steel, were glued to the grip section of the specimens. These tabs were also found to be very effective to reduce the tendency of buckling under fully reversed cyclic loading.

Operation

The MTS 880 system was operated by a standard input, via an external function generator, in the form of a standard +/- 10 V Sine wave function at a frequency of 5-10 Hz. For our first set of experiments i.e, to characterise the hardening behavior as well as the cyclic stress-strain response of DS-Nickel, we chose the strain channel as the active control mode whereas for our second set of experiments i.e, fatigue life measurements, we chose load control as the active mode.

The characterisation of the cyclic hardening curve required cycling at a constant plastic strain amplitude. As the material hardened, a continuous amplitude correction of the total strain was needed to maintain a constant plastic strain amplitude until the material hardened to a steady state. For this purpose, an amplitude correction algorithm was established. While this procedure is best suited for a digital computer, we had to resort to manual control due to the unavailability of a compatible system. The amplitude correction algorithm (Grummon, 1986) can be described as follows,

$$V_{n+1} = V_n \left[1 - \left(\epsilon_m^{pl} - \epsilon_t^{pl} \right) / \left(\epsilon_{max} - \epsilon_{min} \right) \right] \quad .. \quad (7)$$

where

V_{n+1} = Corrected driving signal in the active mode

V_n = Current driving signal in the active mode

ϵ_m^{pl} = Measured plastic strain range in current cycle

ϵ_t^{pl} = Target plastic strain range

ϵ_{max}, ϵ_{min} = Measured max. and min. algebraic values of total strain in the current cycle.

The total strain and the plastic strain was measured in each cycle from the hysteresis loop and the total strain amplitude was modified using the above equation. The process proved very tedious and obviously required some trial and error procedure. However, it was possible to establish a sequential loading pattern which would result in a constant predetermined plastic strain.

The first set of tests involved characterising the cyclic hardening behavior of unmodified and modified DS-Nickel. The specimens were cycled at 0.1 Hz at a constant plastic strain range of 0.0003. The amplitude correction algorithm was used to maintain constant plastic strain.

The second set of tests were designed to characterise the cyclic stress-strain behavior of unmodified and modified DS-Nickel. These "Incremental step tests" were run under strain control and established loading patterns were employed under varying predefined plastic strain. The results were presented in the cyclic stress-strain (CSS) plot, which is

an analog to the monotonic stress-strain diagram. The CSS plots for both the unmodified and modified DS-Nickel were generated.

The third and final set of experiments involved fatigue life determination of unmodified as well as modified specimens. These tests were run under load control. The steady-state stress amplitude for a predetermined plastic strain was obtained from the CSS curves and an established loading pattern was employed to avoid any excessive plastic strain. These tests were run at a higher frequency of 5 Hz to cut down the testing time. The specimens were cycled under fully reversed loading until a fatigue crack was visible. Also these tests were interrupted at every 10,000 cycles to extract the surface replicas for post-fatigue studies. The surface features of the specimen were recorded by means of thin cellulose replicating tape which were moistened with acetone and then pressed against the specimen surface for about 30 seconds. The cellulose tape dissolves in acetone and flows over the surface to create an exact replica which was slowly peeled off and preserved.

Post-Fatigue Surface Characterisation

The surface characterisation of the fatigued specimens involved microscopic observation of the specimen surface under phase contrast optical microscope as well as scanning

electron microscope. To observe the very fine features that may not be resolved under scanning microscope, two-stage surface replicas were extracted at different stages of the test and those were observed under high-voltage transmission electron microscope.

The main objective of these surface studies was to look for any distinct feature such as the development of persistent slip bands and their morphologies. Since fatigue cracks are known to initiate at persistent slip bands, their presence and morphologies could provide informations in regard to the fatigue crack initiation and eventual failure.

The extraction of two-stage carbon replicas involved at first, replication of the specimen surface "in-situ" at different stages of the test. This was done with thin cellulose replicating tape, wetted by acetone and pressed against the surface. As the acetone dried, the tape was slowly peeled off after a few minutes and then it was sputter-coated with carbon under high vacuum. To get better resolution, we used co-deposition of carbon and platinum using the Carbon-Platinum arc points. These carbon coated replicas were then vapor-washed in acetone to dissolve out the cellulose backing, leaving a thin positive carbon replica. These were then observed under transmission electron microscope.

CHAPTER IV

RESULTS

Presentation of the results will be divided into several areas: cyclic strain hardening behavior, cyclic stress-strain behavior, and fatigue life performance. Quite often the results are presented in a comparative format, where the performance of the unmodified and modified species are compared. Also, the results of the mechanical tests are supplemented by microscopic observation of the surface topography as well as fractography.

Cyclic Strain Hardening Behavior

When cycled at a constant plastic strain amplitude of 1.5×10^{-4}, DS-Nickel rapidly hardens to a saturation stress level of 315 MPa with an accumulated plastic strain of 0.03-0.04, which corresponds to about 50 cycles. This rapid cyclic hardening is an important characteristic of this material and is typical of the dispersion strengthened alloys. No cyclic softening is observed after saturation. With the application of Al ion implantation, cyclic hardening behavior is not significantly altered, although a slight increase in the saturation stress level is observed. This issue is discussed later. The typical cyclic hardening behavior of DS-nickel is shown in Figure 4.

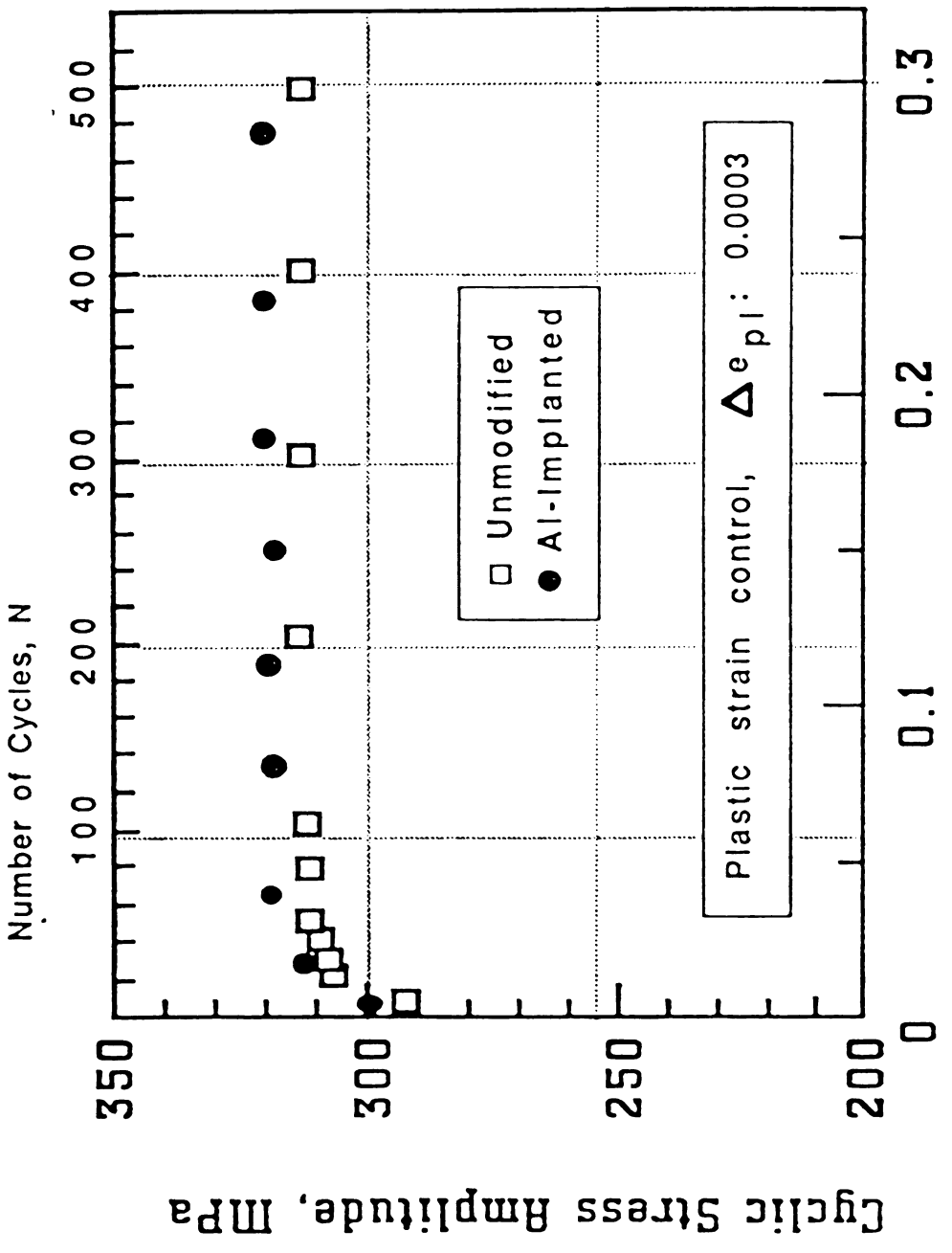

Fig.4 : Cyclic Hardening Behavior of DS-Nickel

Cyclic Stress-Strain Behavior

The cyclic stress-strain behavior of DS-Nickel is presented in the conventional Cyclic stress-strain curves or CSS curves. The saturation stress levels at different plastic strain ranges are recorded under plastic strain controlled cyclic tests. The saturation stress, when plotted against the applied plastic strain range, produces the CSS curve. Due to the buckling tendency of the thin specimens, the plastic strain range for tests in this study was limited to a maximum of 0.001. The CSS curve shows a power law type hardening behavior. The general nature of the CSS curve of DS-Nickel remains more or less unaltered after Al ion implantation, however there is a small increase in the saturation stress levels over the entire range of plastic strain amplitudes. The average increase in the saturation stress level, in this range of plastic strain amplitudes, is about 22 MPa, which is about a 7% increase. Figure 5 shows the CSS curves of the unmodified as well as modified DS-Nickel. Table 2 and Table 3 summarises the test parameters (cyclic stress and plastic strain amplitudes) used to characterise the CSS behavior of modified and unmodified DS Nickel.

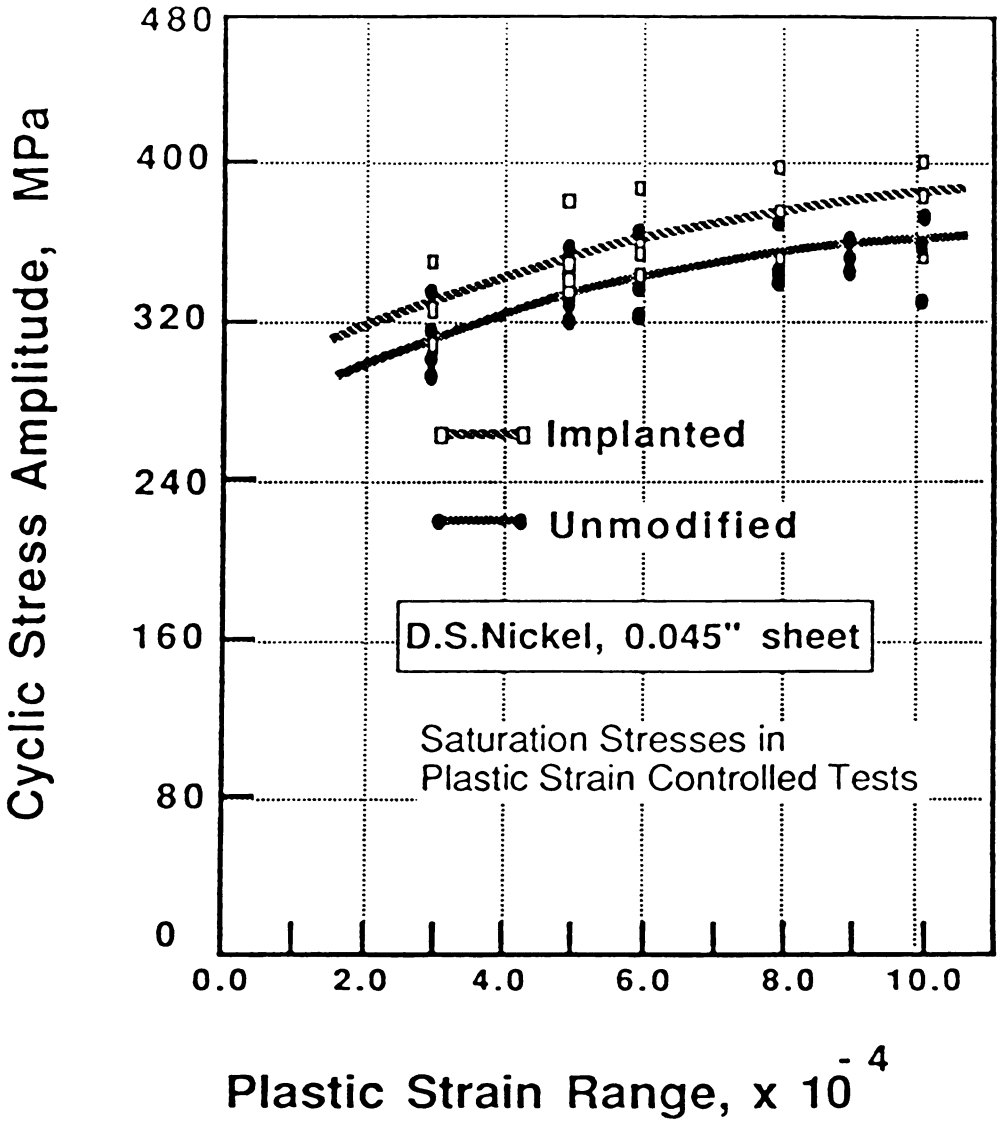

Fig. 5 : Cyclic Stress-Strain Behavior of DS-Nickel

Table 2 : Cyclic Stress-Strain Data for Unmodified DS-Nickel

Specimen Description	Gauge area (sq. mm.)	Plastic Strain	Stress Amplitude	Elastic Modulus
B9/US	9.2512	0.0001	264.4 (MPa)	158.78 (GPa)
B9/US	9.2512	0.0003	314.9	156.61
B9/US	9.2512	0.0006	338.9	157.06
B9/US	9.2512	0.0009	355.8	154.94
B9/US	9.2512	0.002	401.4	155.38
B10/US	8.8228	0.001	373.3	177.97
B11/US	8.9746	0.0003	305.1	148.33
B11/US	8.9746	0.0005	322.1	148.33
B11/US	8.9746	0.0006	330.6	148.33
B11/US	8.9746	0.0008	334.6	148.33
B11/US	8.9746	0.001	337.0	148.33
C3/US	9.0735	0.0003	305.6	161.79
C3/US	9.0735	0.0006	333.11	161.79
C3/US	9.0735	0.0008	347.58	161.79
C3/US	9.0735	0.0005	335.81	161.79
C3/US	9.0735	0.0009	362.28	161.79
C4/US	9.016	0.0003	320.6	—
C6/US	9.2196	0.0003	325.6	169.31
B12/US	8.742	0.0003	325.6	—

Table 3 : Cyclic Stress-Strain Data for Modified DS-Nickel

Specimen Description	Gauge area (sq. mm.)	Plastic strain	Stress Amplitude	Elastic Modulus
C1/1S	9.161	0.0003	320.4(MPa)	164.42(GPa)
C1/1S	9.161	0.0005	346.4	164.42
C1/1S	9.161	0.0006	352.7	164.42
C1/1S	9.161	0.0008	363.6	164.42
C1/1S	9.161	0.001	367.0	164.42
C1/1S	9.161	0.0011	390.5	164.42
C2/IS	8.708	0.0003	314.1	140.25
C2/IS	8.708	0.0005	341.2	140.25
C2/IS	8.708	0.0006	347.3	140.25
C2/IS	8.708	0.0008	355.0	140.25
C2/IS	8.708	0.001	357.5	140.25
C2/IS	8.708	0.0011	352.4	140.25
C5/IS	9.174	0.0003	334.5	169.96
C5/IS	9.174	0.0005	358.8	165.75
C5/IS	9.174	0.0006	373.3	165.8

Low-Cycle Fatigue Behavior

The low-cycle fatigue behavior of DS-Nickel was characterised by cycling under stress control at various stress amplitudes which correspond to a plastic strain range of 0.0001 to 0.001. The results of the fatigue life tests of unmodified DS-Nickel are summarised in Table 4. The number of cycles to failure (N_f) is plotted against the applied stress amplitude (σ_a) on a logarithmic plot (Figure 6). The data for the unmodified material show a linear characteristic according to the Basquin Equation,

$$\sigma_a = \sigma_f' (2N_f)^b \quad \ldots (8)$$

σ_a = Stress amplitude

N_f = Cycles to failure

σ_f' = Fatigue strength coeff.

b = Fatigue strength exponent

For unmodified DS-nickel, σ_f' and b are 1026.0 MPa and - 0.11 respectively. Due to the unavailability of sufficient number of specimens, it was not possible to compute the value of these parameters for modified DS-nickel.

The effect of Al ion implantation on the fatigue life of DS-Nickel was evaluated by subjecting the surface-modified DS-Nickel specimens to similar cyclic stress. However, due to the unavailablity of large number of modified specimens,

Table 4 : Fatigue life data for Unmodified DS-Nickel

Specimen Description	Gauge area (sq. mm.)	Stress Amplitude	Plastic strain	Cycles to failure
D1/UH	12.963	265.9 (MPa)	0.0001	78,498
D3/UH	14.426	285	0.0003	48,326
D6/UH	13.037	305	0.0003	33,592
D7/UH	13.695	319	0.0003	37,665
D9/UH	13.991	380	0.001	5,495
E1/UH	13.584	362	0.001	5,643
E2/UH	14.444	375	0.001	8,152
E3/UH	13.978	382.5	0.001	3,995
E6/UH	14.930	309.5	0.0003	32,072
E7/UH	13.815	314.8	0.0003	25,196
E8/UH	14.575	315.0	0.0003	27,395
E9/UH	13.936	315.3	0.0003	35,778
E11/UH	14.762	314.8	0.0003	35,175
E12/UH	14.777	315.4	0.0003	25,445
E13/UH	14.998	314.9	0.0003	20,012

it was not feasible to employ various levels of stress amplitude. Instead, a single stress amplitude (315 MPa) was chosen, which corresponded to a plastic strain range of 0.0003. The results of the fatigue life tests of modified DS-Nickel are summarised in Table 5. The average number of cycles to failure for surface-modified DS-Nickel at this stress amplitude was significantly higher than that of unmodified DS-Nickel. These results are incorporated in Figure 6 to show the comparatively higher fatigue lives of modified DS-Nickel. Due to the inherent scatter in the fatigue test data, it was necessary to perform a statistical analysis on these data and based on that analysis, it can be concluded with more than 80% confidence that the mean life of the modified DS-Nickel specimens is significantly higher than that of the unmodified specimens (see Appendix I).

The average life of unmodified DS-Nickel, under a constant plastic strain range of 0.0003, is about 28,000 cycles, whereas the average life of modified DS-Nickel under similar plastic strain is about 36,000 cycles. This corresponds to a 28% increase in fatigue life. This result is in line with the results of similar work by other investigators (Jones & Morrison, 1987). Table 6 summarises the effect of Al ion implantation on the fatigue lives of pure Nickel as well as DS-Nickel.

Table 5 : Fatigue Life Data for Modified DS-Nickel

Specimen Description	Gauge area (sq. mm.)	Stress Amplitude (MPa)	Plastic Strain range	Number of cycles to failure
D2/IH	13.852	315.0	0.0003	33,116
D10/IH	13.905	315.0	0.0003	24,825
D11/IH	14.860	315.2	0.0003	38,425
D8/IH	13.977	315.5	0.0003	59,641

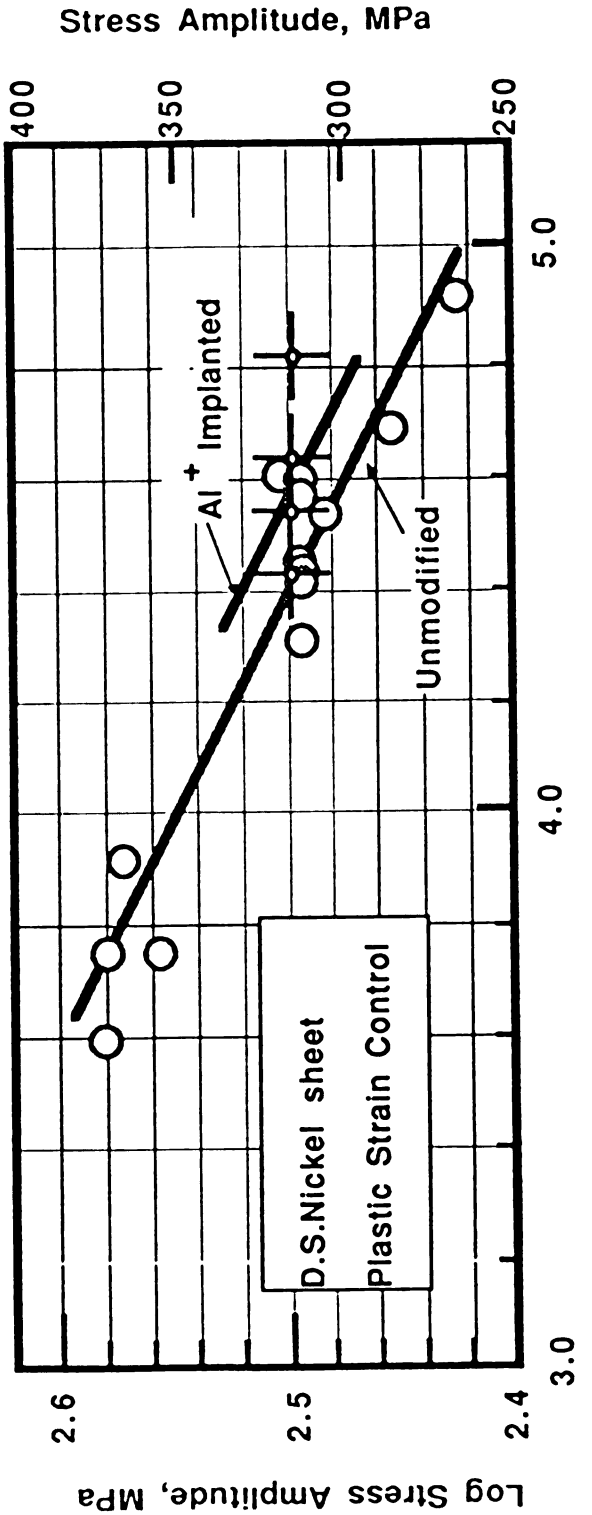

Fig. 6 : Fatigue Life Performance of DS-Nickel

Table 6 : Comparison of Fatigue Life of Pure Nickel and DS-Nickel with and without Aluminum Ion Implantation

MATERIAL	PLASTIC STRAIN RANGE	CYCLES TO FAILURE		INCREASE IN FATIGUE LIFE (%)
		UNMODIFIED	AL - ION IMPLANTED	
Pure Nickel , Coarse grains *	5×10^{-4}	49,750	70,500	42
Pure Nickel , Fine grains *	5×10^{-4}	219,000	279,000	27
ThO_2 DS- Nickel	3×10^{-4}	28,000	36,000	28

* Jones and Morrison, 1987

The results presented so far contain the results of various mechanical tests that were performed to characterise the effects of Al^+ ion implantation on the cyclic plasticity behavior of DS-Nickel. To supplement the results of these mechanical tests, microscopic observation of the specimens were performed, which is detailed below.

Microscopic Observation of the Specimens

The microscopic observation of the specimens comprised of: a) Nomarski phase contrast optical microscopy;
b) Observation of the fracture surface and the specimen surface under the scanning electron microscope and
c) Observation of the two-stage carbon surface replica under transmission electron microscope.

The main objective of the microscopic observation of the specimen surface was to find if there was any formation of persistent slip bands, which are known to initiate fatigue cracks. Also, if there were any formation of persistent slip bands, the ion implantation would have altered the morphology of these bands and that would give some clue to the micromechanism of fatigue crack initiation in DS-Nickel. The morphology of the PSB, particularly with respect to the formation of deep extrusions/intrusions, dictate to a large extent whether the crack is initiated within the PSBs or at PSB-matrix interface.

The first set of microscopic observations consisted of studying the electropolished surfaces of the specimens using Nomarski phase contrast microscopy, before and after fatigue. It was observed that there were no formation of slip bands in unmodified DS-Nickel. No other evidence of surface damage accumulation could either be resolved under optical microscopy (Figure 7). The absence of any slip band formation in fatigued DS-Nickel was unexpected, but not quite surprising. As discussed earlier, PSB formation is mostly favoured by a single active slip system. However, in DS-Nickel, the presence of very fine ($\approx$ 25 nm) thoria particles causes the homogenisation of plastic strain by activating multiple slip systems near their vicinity. The effect of plastic strain homogenisation is so pronounced that no slip bands could be observed, at least with the optical microscope. The surface of the modified DS-Nickel was also observed before and after fatigue, but there was hardly any surface damage feature that could be resolved with optical microscope (Figure 8), except the fine sputtering morpholgy resulting from ion implantation. However looking at the crack tip (Figure 9),it was observed that there were considerable surface damage near the crack tip, but only in the form of surface rumplings.

The next step was to observe the specimen surface and the fracture surface under the scanning electron microscope. The specimen surfaces were observed before and after fatigue but

no prominent surface features were found that could be related to fatigue crack initiation. However, an exception to this general pattern was observed at the edges of the thin sheet specimens, where PSB formations did take place (Figure 10). There was no severe extrusion/intrusion formation within the PSB (Figure 11) and crack initiation was found to occur at the PSB-matrix interface (Figure 12). In other cases, however, crack initiation was often found to occur without any appreciable surface damage in the form of slip bands (Figure 13) and it was speculated that a mechanism of sub-surface crack initiation may be operative. Upon observation of the modified specimens, it was found that there was no formation of surface slip bands in the regions that were fully exposed to the ion beam. Again cracks were found to initiate in these specimens at the edges, which may not have received full radiation dose (Figure 14 & 15).

The fracture surfaces were examined under SEM to determine the possible crack initiation site. The fracture surfaces were found to contain numerous microcracks all over the matrix (Figure 16). The presence of these small cracks suggest that the failure may have resulted from a sub-surface fatigue crack initiation. This issue is discussed at length in later sections.

The final technique used in surface observation was to replicate the finest surface features of the specimen and to

observe the replicas under very high magnification. The procedure of creating two-stage carbon replicas has already been discussed previously. These carbon replicas were observed under transmission electron microscope under very high magnification (X 400,000). Observations at this high magnification confirmed the findings mentioned earlier.

In summary, it has been observed that in fatigued, unmodified DS-nickel, slip bands do not appear for most of the surface area. However, slip bands have been observed at the edges of sheet specimens. When slip bands are present, crack initiation usually takes place at the PSB-matrix interface. However, quite often, cracks are initiated in the absence of any slip bands and in those cases, a sub-surface crack initiation mechanism is speculated. In fatigued, modified DS-nickel specimens, slip band formation was completely suppressed in the regions which received full radiation dose. However, slip band formation and crack initiation was found to take place at the edges of sheet specimens, which may not have received full radiation dose.

Electropolished Surface
Before Fatigue Loading

Surface After
Fatigue to Failure

500 x

Fig. 7 : Unmodified DS-Nickel Specimens

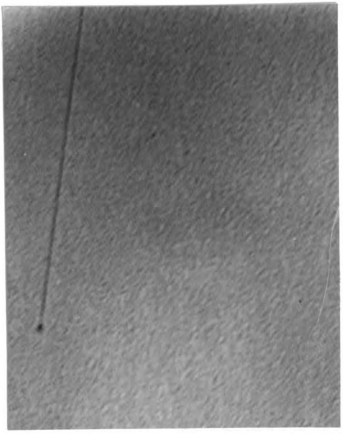

Electropolished Surface
Before Fatigue Loading

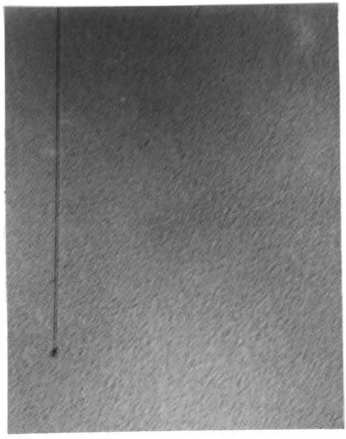

Surface After
Fatigue to Failure

500 x

Fig. 8 : Al Implanted DS-Nickel Specimens

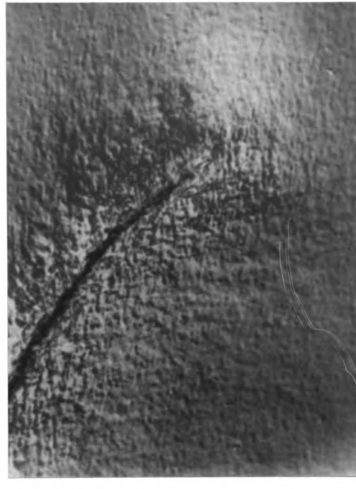

Fig. 9 : Crack Tip Morphology in DS-Nickel

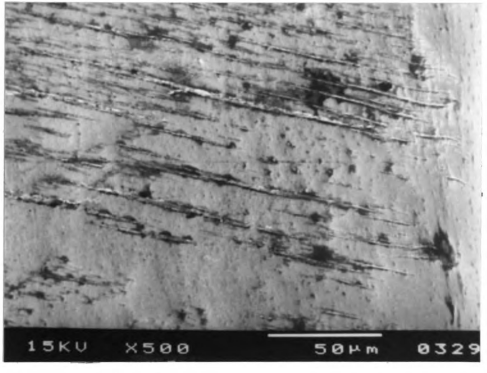

Fig. 10 : Slip Band Formation at the Edges of Unmodified DS-Nickel Sheet Specimens

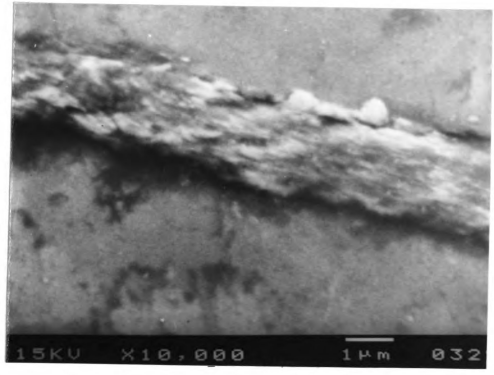

Fig. 11 : Surface Morphology of a Slip Band Formed in Unmodified DS-Nickel Specimen

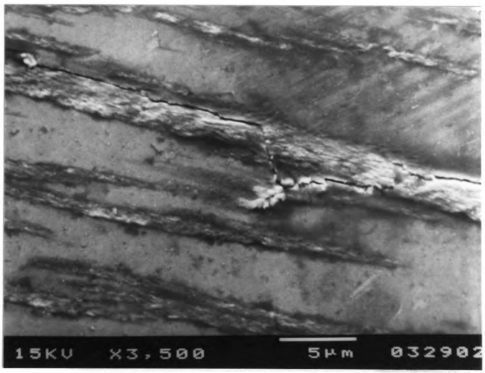

Fig. 12 : Fatigue Crack Initiation at the PSB-Matrix Interface in Unmodified DS-Nickel

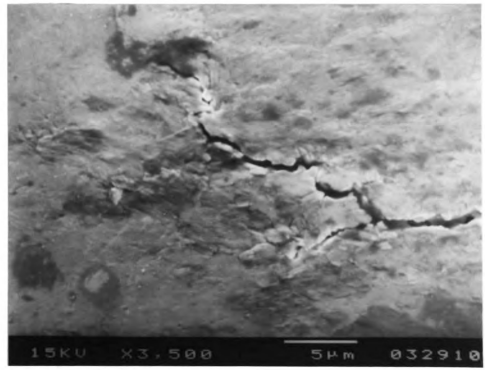

Fig. 13 : Fatigue Crack Formation in Unmodified DS-Nickel, without Appreciable Presence of Slip Bands

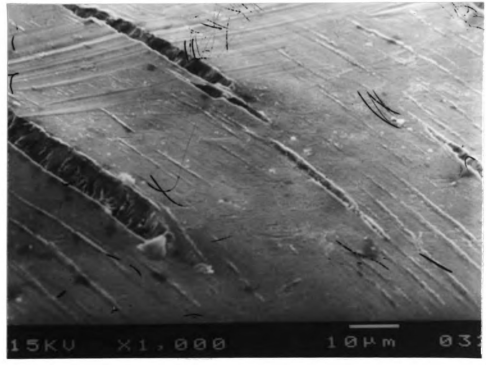

Fig. 14 : Persistent Slip Band Formation and Fatigue Crack Initiation at the Edges of Surface Modified DS-Nickel Specimens

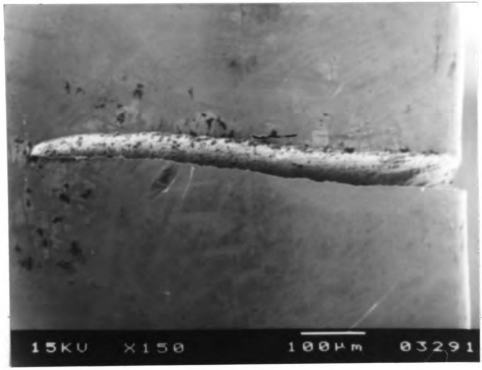

Fig. 15 : Fatigue Crack Initiated at the Edges of Surface Modified DS-Nickel Specimens

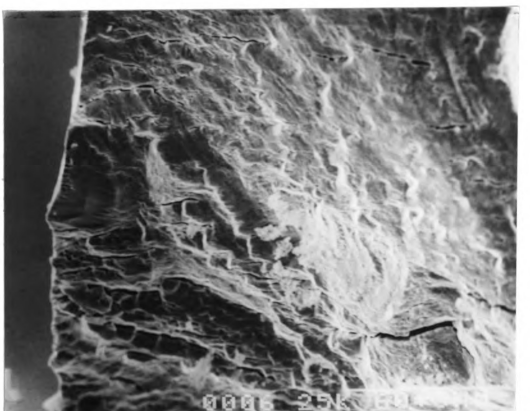

Fig. 16 : Fracture Surface of Unmodified DS-Nickel, Showing the Profusion of Micro-cracks in the Matrix

CHAPTER V

DISCUSSION

In this section, various results of the experiments that were presented in earlier sections will be critically analysed and the implications of those results will be discussed.

The results presented in the previous chapter may be summarised as follows:

(a) DS-Nickel shows rapid cyclic hardening behavior and ion-implantation does not significantly affect its rate of hardening.

(b) Aluminum ion-implantation causes a 7% increase in the saturation stress level of DS-Nickel within a range of plastic strain amplitudes of 1.5×10^{-4} - 5.0×10^{-4}.

(c) Aluminum ion-implantation causes a 28% increase in the fatigue life of DS-Nickel at a stress amplitude of 315 MPa.

(d) For the range of plastic strain amplitudes employed in this study, DS-nickel, for the most part, does not show any evidence of slip band formation during fatigue. However,

slip bands were found to appear at the edges of sheet specimens and initiated fatigue cracks at the PSB-matrix interface.

(e) Surface modification of DS-nickel by ion-implantation was found to completely suppress the appearance of slip bands in the regions which received full radiation dose. Slip bands and consequent fatigue cracks did appear at the edges of sheet specimens, which were probably shadowed during ion implantation process.

In light of these observations, let us now analyse and explain each of these findings.

Cyclic Deformation and Plasticity Behavior

DS-Nickel showed a very rapid cyclic hardening tendency and it reached the saturation stress in less than 100 cycles. This behavior is typical for dispersion strengthened alloys and this rapid rate of hardening is attributed to the presence of very fine dispersoids which causes dislocation "pile-up"s and activates multiple slip systems in their vicinity due to cross-slip of the dislocations. The rate of cyclic hardening of DS-Nickel was not significantly altered by aluminum ion implantation and this is probably due to the fact that the cyclic hardening rate of DS-Nickel is governed mainly by the size and distribution of the thoria particles

which remains unaltered during ion implantation.

The small but noticeable increase in the saturation stress levels of DS-Nickel after ion implantation is apparent from the CSS curves. In fact, the saturation stress level was increased by about 7% in the appplied plastic strain range. It is theorised that the hard surface layer act as a barrier to dislocation motion during cyclic deformation and results in a pile-up of dislocations in the near-surface region. This dislocation pile-up, in turn gives rise to a back-stress, which results in an increase in the stress amplitude for a prescribed plastic strain. However, this effect may have a direct dependence on the ratio of the modified surface area to the total cross-sectional area of the specimen.

The increase in the low-cycle fatigue life of DS-Nickel after aluminum ion implantation was expected and is in line with the observations of other researchers (Jones & Morrison, 1987 etc.). A moderate increase in fatigue life (28%) at 315 MPa stress level was observed. The increase in the fatigue life can be explained in terms of accumulated plastic strain during cyclic deformation. As we have noticed before, the ion-implanted surface layer act as a barrier to dislocation glide and result in a lower plastic strain for a prescribed stress level. As a result, when cycled under stress-control and at the same stress amplitude, the ion-implanted specimen would accumulate less plastic strain than

the unimplanted one for equivalent number of cycles. Since failure is initiated at a critical value of accumulated plastic strain, the ion-implanted specimens would survive higher number of cycles before failure. A more detailed explanation of the higher fatigue life of ion-implanted specimens, based on the fracture mechanics concept, will be presented later.

The cyclic plasticity behavior of DS-Nickel is affected due to aluminum ion-implantation. A hard, thin surface layer which results from ion-implantation acts as an obstacle to dislocation motions and thus tend to reduce the extent of plastic deformation. It can be stated with reasonable confidence that the surface layer which results from aluminum ion implantation has higher yield strength than the bulk. This additional hardening effect comes from various factors e.g, introduction of numerous lattice defects due to ion bombardment and solid solution hardening. Some other secondary factors may contribute to the surface hardening and they include, a) formation of accomodation dislocation networks, and b) presence of a residual compressive stress at the surface after ion implantation. Although the effects of these individual factors towards surface hardening cannot be quantified immediately, it can be logicaly assumed that the cumulative effects of all these factors result in a significant surface hardening.

Since the surface layer has higher yield stress, it can

be expected that for very small applied plastic strain, most of the plastic strain will be present in the bulk while the surface layer would essentially cycle elastically and thus the surface would not experience any fatigue damage due to plastic deformation. Another factor that might be beneficial in this context is the elastic modulus effect. If the elastic modulus of DS-Nickel is reduced by surface alloying with aluminum, then the surface would experience lower stress than the bulk. Although there is evidence that aluminum addition does lower the elastic modulus of pure nickel, no such experimental evidence is available for DS nickel, whose elastic modulus is much lower than that of pure nickel. In any case, the elastic modulus effect would be less pronounced than the surface hardening effect. So, for small applied plastic strain range, we will have a situation where the bulk of the specimen undergoes plastic strain while the surface layer essentially suffers little or no plastic strain and cycles elastically. As a result, the surface does not undergo any damage that might have occured due to plastic deformation.

Fatigue Crack Initiation and Failure Mechanism

From the microscopic observation of the fatigued, unmodified DS-nickel specimens, it was apparent that there was hardly any formation of persistent slip bands on most of the free surfaces of the specimens during cyclic

deformation of DS-nickel. The only exception to this general observation was at the edges of sheet specimens, where slip bands did appear and were found to initiate fatigue cracks at the PSB-matrix interface.

It is theorised that in DS-Nickel, for the range of plastic strain amplitudes employed in this study, the presence of very fine thoria particles in the nickel matrix homogenise the plastic strain resulting in a uniform distribution of plastic strain all over the matrix. As a consequence, there is no significant plastic strain localization anywhere in the matrix. This explains the absence of any persistent slip bands in fatigued DS-Nickel.

However, the situation is quite different at the edges of sheet specimens, where the geometrical stress concentration factor can be as high as 1.38 for hourglass specimens (Peterson, 1974). While the hourglass specimen is cycled at a nominal stress amplitude of 315 MPa, the maximum stress at the edges may go upto 435 MPa. From the CSS curve of DS-nickel (Leverant & Sullivan, 1968), it can be seen that this maximum stress at the edges would correspond to a maximum plastic strain amplitude of about 0.016, which is about 100 times higher than the nominal plastic strain amplitude of 1.5×10^{-4}. The direct consequence of this increased plastic strain at the edges of the sheet specimens, is the formation of persistent slip bands in those regions. This observation is in agreement with the findings of Leverant and Sullivan

(1968), who showed evidence of slip band formation in DS-nickel, when cycled at a range of plastic strain amplitudes from 0.002 to 0.015.

It may be argued that for relatively low plastic strain amplitudes (e.g, upto about 5.0×10^{-4}), the plastic strain in DS-nickel is distributed homogeneously over the matrix by the fine thoria particles. While the plastic strain homogenization effect of thoria particles is quite strong at lower plastic strain amplitudes, this process is not quite so effective at higher plastic strain amplitudes. As a result, plastic strain localization occurs, giving rise to the formation of persistent slip bands.

Crack initiation in DS-nickel has often been found without the presence of any apparent slip band formation and this observation leads to the possibility of sub-surface crack nucleation. There have been some reports of sub-surface crack initiation in the past (Vardiman & Kant, 1981), but only in high-cycle fatigue regime. As far as the sub-surface crack initiation site is concerned, the particle-matrix interface seems to be the most probable site. There have been reports of void formation at the particle-matrix interface in monotonic tensile deformation of internally oxidised copper alloys (Palmer & Smith, 1966) and it may be speculated that similar formation of voids at the interface may occur during cyclic loading and could very well act as the crack nucleation site. However, no such hard

evidence is available that would decisively prove the existence of such mechanism.

However, if sub-surface crack initiation is assumed, the increase in the fatigue life observed in the ion-implanted DS-Nickel can be explained, at least on a qualitative basis, from a fracture mechanics point of view. As we know, the stress intensity factor associated with a surface crack is considerably higher than that associated with an interior (sub-surface) crack of the same overall crack length. While the exact relation depends on the loading configuration and crack geometry, it can be stated in general that a surface crack is associated with a higher stress intensity factor than a sub-surface crack. Now in unmodified DS-Nickel, the nucleated crack is a sub-surface one and with continued cycling, it immmediately grows to a free surface and becomes a surface crack. However, in modified DS-Nickel, the hard surface layer resists the growth of the sub-surface crack and forces it to grow in a non self-similar manner. In other words, in early stages of fatigue, the presence of this hard surface layer delays the transformation from sub-surface to a surface (edge) crack. However, once the edge crack is formed, the situation is identical in both the implanted and the unimplanted specimen and the crack grows freely, leading to catastrophic failure. Thus the increase in the fatigue life of the implanted specimen can be solely attributed to the time delay caused by the hard surface layer in the transformation of a sub-surface crack to a surface (edge)

crack.

Analysis of Fatigue Crack Growth

The growth rate of a fatigue crack under low-cycle fatigue condition is given by (Tomkins, 1968),

$$(da / dn) = \Delta\epsilon_p . \Delta D \quad \ldots\ldots (9)$$

where,

$\Delta\epsilon_p$ = the plastic strain range

D = size of the crack-tip plastic zone

$\Delta D = D_{max} - D_{min}$

D_{max} = Plastic zone size at σ_{max}

D_{min} = Plastic zone size at σ_{min}

From Irwin's analysis (Hellan, 1984), the size of the crack-tip plastic zone is given by,

$$D = (1 / \pi k^2) (K_I^2 / \sigma_y^2) ,$$

where, k = 1, for plane stress

k = $\sqrt{3}$, for plane strain

σ_y = yield stress

For our case, we can assume plane stress condition, k = 1.

The stress intensity factor is given by,

$$K_I = \sigma\sqrt{(\pi a)} \ , \quad a = \text{half crack length}$$

So, the crack-tip plastic zone size is given by,

$$D = a(\sigma/\sigma_y)^2$$

Again, $\Delta D = D_{max} - D_{min}$

$$= (a / \sigma_y^2)(\sigma_{max}^2 - \sigma_{min}^2)$$

For a fully reversed cyclic loading, $\sigma_{min} < 0$. As far as the crack growth is concerned, the compressive part ($\sigma<0$) has no significant contribution and thus we can replace it by the lower bound, $\sigma_{min} = 0$.

So, $D_{min} = 0$, and $\Delta D = D_{max} = a(\sigma_{max}/\sigma_y)^2$

For our case,

σ_{max} = 315 MPa, σ_y = 350 MPa and $\Delta\epsilon_p$=0.0003

Thus, $(da/dn) = D_{max}.\Delta\epsilon_p = a\ (2.43 \times 10^{-4})$ mm/cycle.

This gives us the fatigue crack growth rate in unmodified DS-Nickel.

Now for modified DS-Nickel, we have a hard surface layer and let us denote the yield stress of the surface layer by,

$\sigma_y' = \lambda\sigma_y$, where $\lambda > 1$

and σ_y = yield stress of unmodified DS-nickel

So, the fatigue crack growth rate in the modified DS-Nickel is given by,

$$(da/dn)' = \Delta\epsilon_p.(\Delta D)' = \Delta\epsilon_p.a.(\sigma_{max}/\lambda\sigma_y)^2$$

$$= a\ (2.43 \times 10^{-4}) / \lambda^2$$

So, comparing, we get,

$$(da/dn)' / (da/dn) = 1 / \lambda^2$$

We can see from this relation, that the crack growth rate in the surface layer as compared to the bulk, is strongly dependent on its yield stress. For instance, a 15% increase in the surface yield stress of DS-Nickel will result in a 25% reduction in the fatigue crack growth rate in the surface layer.

Low-Cycle Fatigue Life Estimation

Let us recall the fatigue crack growth equation (9),

$$da/dN = \Delta\epsilon_p . \Delta D$$

For our case, $\Delta D = a(\sigma_{max}/\lambda\sigma_y)^2$

where, $\lambda = 1$, for unmodified DS-Nickel

and $\lambda > 1$, for modified DS-Nickel surface layer

So, we get,

$$da/dN = \Delta\epsilon_{pl} . a . (\sigma_{max}/\lambda\sigma_y)^2$$

or, $da/a = \Delta\epsilon_p . (\sigma_{max}/\lambda\sigma_y)^2 \, dN$

Integrating, we get,

$$\ln (a_c/a_o) = C / \lambda^2 \, (N_f - N_o)$$

where

$C = \Delta\epsilon_p . (\sigma_{max}/\sigma_y)^2$

a_o = initial crack length

a_c = final (critical) crack length

N_o = Number of cycles for crack initiation

N_f = Number of cycles to failure

Rewriting, we get,

$$N_f = N_o + (\lambda^2/C) \ln (a_c/a_o) \quad .....(10)$$

This is the generalised low-cycle fatigue life equation.

For unmodified DS-Nickel, this equation can be directly used to either solve for the critical crack size (a_c) or to predict the fatigue life for a pre-defined crack size.

The number of cycles for crack initiation, N_o, is typically assumed to be about 10% of the total fatigue life, N_f.

For unmodified DS-Nickel,

$$N_f = 28{,}000 \ , \quad N_o = 0.1N_f = 2{,}800$$
$$C = 2.43 \times 10^{-4} \ , \quad \lambda = 1$$

So, from eqn. (2) , we get, $a_c = 456.5\ a_o$

This relation can be later used to predict the fatigue life of modified DS-Nickel.

Prediction of Low-Cycle Fatigue Life of Modified DS-Nickel

The total fatigue life of a specimen can be subdivided into three parts, e.g, (a) the time to initiate a flaw or crack ; (b) the growth of the initial crack to a threshold value where rapid growth of the crack takes over; and (c) the rapid growth of the crack to a catastrophic failure.

Mathematically,

$$N_f = N_i + N_c + N_g$$

where

N_f = total fatigue life to failure (# of cycles)

N_i = time to initiate a flaw (,,)

N_c = growth of the initial flaw to a threshold size (,,)

N_g = rapid growth period (,,)

Typically, N_i is assumed to be about 10% of the total life (i.e, $N_i \approx 0.1\ N_f$). The most critical parameter is N_c, the time taken for the initial flaw to grow to a threshold size when the rapid growth sets in. For modified DS-Nickel, this period denotes the growth of a sub-surface sub-micron crack through the hard surface layer to become an edge crack.

So, for modified DS-Nickel,

$$N_c = d \,/\, (da/dn)'$$

where , d = thickness of the hard surface layer

and $(da/dn)'$ = crack growth rate in the surface layer

Recall that, $(da/dn)' = (1/\lambda^2)(da/dn)$

and also, $da/dn = a\ (2.43 \times 10^{-4})$ mm/cycle.

If we assume, a = 50 nm , d = 300 nm and $\lambda = 1.15$ then,

we get, N_c = 32,654 cycles

As mentioned before, N_i is assumed to be about 10% of total life, N_f. For unmodified DS-Nickel, N_i = 2,800 cycles. We can use this same value of N_i for modified DS-Nickel, because the flaw initiation is a bulk process, which remains unaltered during surface modification.

The final failure occurs due to the rapid growth of the crack. This period is denoted by N_g and for modified DS-Nickel, we get,

$$N_g = N_f - N_c - N_i$$
$$= 36,000 - 32,654 - 2,800$$
$$= 546 \text{ cycles}$$

As we can see, the majority of the fatigue life of modified DS-Nickel is spent during the slow growth of the sub-surface crack through the ion-implanted surface layer.

Based on this observation, we can define an effective crack growth rate for modified DS-Nickel from a simple rule of mixture concept as follows,

$$(da/dn)_{eff} = (N_c/N_f)(da/dn)' + (N_g/N_f)(da/dn)$$

If we assume, a = 50 nm, d = 300 nm and λ = 1.15,

we get, for modified DS-Nickel,

$$(da/dn)_{eff} = 8.38 \times 10^{-9} \text{ mm/cycle}$$

Furthermore, if we assume this effective crack growth rate to be representative of the modified DS-Nickel, then, as in unmodified DS-Nickel, we can integrate the crack growth rate equation over the whole range of crack growth and solving as before, we get the fatigue life eqn. (10),

$$N_f = N_o + (\lambda^2/C) \ln (a_c/a_o)$$

Here, $N_o = 2800$, $C = 2.43 \times 10^{-4}$ and $\ln (a_c/a_o) = 6.12$,

So, for ion-implanted DS-Nickel, we get,

$$N_f = 2800 + \lambda^2 [6.1236 / (2.43 \times 10^{-4})]$$

If we assume, $\lambda = 1.15$, we get $N_f = 36,127$ cycles

This predicted value of N_f for modified DS-Nickel agrees very well with the experimental value of 36,000 cycles. Thus, based on these calculations, it can be speculated that the surface modification of DS-Nickel by ion-implantation creates a hard surface layer which has a yield strength about 15% higher than the bulk and this hard surface layer is instrumental in slower crack growth rate, therby causing a 28% increase in the fatigue life.

Prediction of Initial Flaw Size in DS-Nickel

So far, it has been postulated that the increased fatigue life in the ion-implanted DS-Nickel is due to the slower crack growth through the hard surface layer. Now let us recall from earlier discussion that,

$$N_f = N_i + N_c + N_g \text{ , for unmodified DS-Nickel}$$

$$\text{and } N_f' = N_i + N_c' + N_g \text{ , for modified DS-Nickel}$$

As discussed before, the bulk properties of DS-Nickel remains unaltered during surface modification and thus we can assume N_i and N_g, which are related to the bulk properties, to remain unaltered.

Also recall that,

$$N_c = d / (da/dn) \quad \text{and} \quad N_c' = d / (da/dn)'$$

where,

d = the thickness of the surface layer

So, we get,

$$N_c' - N_c = N_f' - N_f = 36,000 - 28,000 = 8,000$$

$$\text{but, } N_c' = N_c [(da/dn) / (da/dn)'] = \lambda^2 N_c$$

or, $(\lambda^2 - 1) N_c = 8,000$

If we assume, $\lambda = 1.15$, then $N_c \approx 24,800$

Now, $(da/dn) = d / N_c$

here, $d = 300$ nm and $N_c \approx 24,800$

thus, $(da/dn) \approx 1.2 \times 10^{-8}$ mm/cycle

Also, we know for low-cycle fatigue,

$$(da/dn) = \Delta\epsilon_p . \Delta D$$

here, $\Delta\epsilon_p = 0.0003$ and $\Delta D = 0.81a$

So, we have,

$$(0.0003)(0.81a) = 1.2 \times 10^{-8}$$

or, $a \approx 50 \times 10^{-6}$ mm = 50 nm

Thus, the initial flaw size in DS-Nickel is calculated to be of the order of 50 - 100 nm.

Experimental evidence of void formations at the particle-matrix interface in internally oxidised copper alloys had been reported by Palmer and Smith (1966). The voids, at an early stage of formation, at the Cu - SiO_2 interface, were

measured to be of the order of 50 - 70 nm. Thus our theoritical prediction of initial flaw size agrees quite well with the experimental observations.

To summarize, a detailed analysis, based on fracture mechanics concepts, has been carried out to quantify the effect of a thin, hard surface layer on the low-cycle fatigue life. The analysis predicts a fatigue life of 36,127 cycles for the modified DS-nickel specimens, which is very close to the observed fatigue life of 36,000 cycles, on the basis of an assumed 15% increse in the yield stress of the surface layer over the bulk. This assumption of 15% increase in the yield stress of the surface layer seems quite reasonable, although there is no experimental data to support this assumption.

However, a questionable prediction of this analysis is the initial flaw size, which according to this analysis, comes out to be of the order of 50-100 nm. This value is much smaller than the typically quoted initial flaw size of 25-50 μ. This raises the fundamental question of the applicability of such an analysis based on fracture mechanics, to such a small size flaw. The situation is even more complicated by the fact that the applied stress amplitude is very close to the gross yield stress and elasto-plastic fracture mechanics analysis cannot properly describe such situations. A more fundamental analysis, either based on dislocation theory or strain energy methods

may be more appropriate. However, to date there is no such single established analysis available that can be directly applied in such a situation.

CHAPTER VI

CONCLUSIONS

High energy aluminum ion implantation has been found to be a useful technique to modify the surface of thoria dispersion strengthened nickel by producing a thin, hard surface layer. Using this method, it was possible to create specific surface conditions which would otherwise be difficult, if not impossible to produce.

The cyclic plasticity behavior of DS-Nickel with and without surface modification by aluminum ion implantation was characterised. It was observed that DS-Nickel undergoes rapid cyclic hardening and aluminum ion implantation did not significantly affect its rate of hardening. It was concluded that ion implantation which only alters the surface does not affect the bulk properties of the substrate.

The saturation stress levels of ion-implanted DS-Nickel showed a small increase compared to that of unmodified DS-Nickel, as measured in the cyclic stress-strain behavior under constant plastic strain tests. This small increase is attributed to the presence of the hard surface layer, which acts as a barrier to dislocation glide, thereby causing a hardening effect.

The low-cycle fatigue life of DS-Nickel was moderately increased by surface modification by aluminum ion implantation, as measured under stress controlled fatigue tests. The presence of a hard surface layer in ion-implanted DS-Nickel reduced the extent of plastic deformation by acting as a barrier to dislocation motion and therefore contributed to the increased fatigue life.

From the macroscopic and microscopic observation of the surface of cyclically deformed specimens of DS-Nickel, it was concluded that for the range of plastic strain amplitudes employed in this study, DS-Nickel does not develop persistent slip bands on most of its free surfaces during cyclic deformation. Only exception to this pattern was found at the edges of sheet specimens, where slip bands did form and were found to initiate fatigue cracks at the slip band-matrix interface. The stress concentration at the edges of sheet specimens was high enough to produce very large plastic strain amplitude and as a result, persistent slip bands were formed in these regions. This observation is in agreement with the findings of an earlier work by Leverant and Sullivan (1968).

Often, fatigue cracks were found to initiate without apparent surface damage in the form of slip bands and it was concluded that a mechanism of sub-surface crack nucleation was active in this system. It was speculated that the crack may have initiated at the particle-matrix interface.

Assuming that sub-surface crack nucleation occured, the effect of the hard surface layer in the ion-implanted DS-Nickel towards the increase of fatigue life was explained from a fracture mechanics point of view. The presence of the hard surface layer reduces the crack growth rate in the early stages of fatigue and delays the transformation of a sub-surface crack to a surface crack. This delay is manifested in the increased fatigue life of modified DS-Nickel.

It must be noted, however that the fracture mechanics analysis employed here does have some severe limitations. A more fundamental analysis based on either dislocation theory or strain energy methods may be more appropriate.

Scope of Future Research

The present work was directed to investigate and provide a better understanding of the cyclic deformation behavior of dispersion strengthened nickel alloyand the associated effects of aluminum ion implantation, as a continuing effort to understand the complex mechanisms associated with the presence of an ion implanted surface layer and the underlying cyclically deforming substrate. The present work

has also demonstrated the potential of ion implantation process as a tool to modify the surface of a dispersion strengthened alloy to improve its low-cycle fatigue performance. A model has been proposed to characterise the cyclic deformation behavior of DS-Nickel which is consistent with the observations. However, it has also raised a few interesting questions which could provide the guidelines for further research in this area.

First of all, it has not been possible to pinpoint the exact location of the sub-surface fatigue crack initiation. It has been speculated that the crack might have initiated at the particle-matrix interface, however further research is needed, particularly involving extensive transmission electron microscopy, to conclusively settle this issue.

Also, due to the limitation on the specimen geometry, it has not been possible to characterise the cyclic stress-strain behavior of DS-Nickel at higher plastic strain ranges. Future work in this direction will provide some useful informations which will give a more comprehensive picture of the physical processes.

Another limitation of the present work was that the low-cycle fatigue tests of the modified DS-Nickel were carried out at only one stress level. It will be useful to carry out similar fatigue tests at higher stress levels which would give better comparison of fatigue lives between the

unmodified and modified DS-Nickel.

Also, to quantify the effects of ion implantation on fatigue life, a fracture mechanics based analysis has been presented. Although, in this case, the theoritical prediction comes very close to the experimental observations, the theory does suffer from severe limitations. A more fundamental approach, based on dislocation theory or strain energy methods would be more appropriate.

Finally, future research on similar dispersion strengthened alloys will be of interest. In particular, research on aluminum and copper base dispersion strengthened alloys and particulate-reinforced composites which are of considerable commercial importance, will be very much in order.

APPENDIX

APPENDIX I

Statistical Analysis of Fatigue Life Data

The low-cycle fatigue life of surface modified DS-Nickel was found to be higher than that of unmodified DS-nickel, as determined under stress controlled fatigue tests at an amplitude of 315 MPa. However, due to the inherent scatter in the data, it was necessary to perform a statistical analysis to determine the confidence level at which the mean fatigue life of surface modified specimens was significantly higher than that of unmodified DS-Nickel. The "Student T-Distribution" method was used to determine the confidence level at which the difference between the two mean values was statistically significant.

Experimental Data

Unmodified Specimens

Number of samples, $n_x = 6$

Mean fatigue life, $\mu_x = 28,166$

Standard deviation, $S_x = 6,170$

Surface Modified Specimens

Number of samples, $n_y = 2$

Mean fatigue life, $\mu_y = 35,770$

Standard deviation, $S_y = 3,754$

Statistical Analysis

(Ref: Engineering Experiments, Lipson & Sheth, 105)

We compute,

$$\nu = n_x + n_y - 2 = 6$$

$$A = [\{ (n_x-1)S_x^2 + (n_y-1)S_y^2 \}\{ n_x + n_y \} / \{ \nu\, n_x\, n_y\}]^{1/2}$$

$$= 4766$$

and, $t_2 = (\nu_x - \mu_y) / A = -1.595$

Now, for 80% confidence level, $\alpha/2 = 0.1$

and from t-distribution table, $t_{0.1,\ 6} = 1.440$

Also, for 90% confidence level, $\alpha/2 = 0.05$

and from t-distribution table, $t_{0.05,\ 6} = 1.943$

Since, $1.440 < ABS(t_2) < 1.943$

We can say with more than 80% confidence that the average fatigue life of surface modified DS-Nickel is significantly higher than that of unmodified DS-Nickel.

BIBLIOGRAPHY

BIBLIOGRAPHY

1) Abel, A. & Ham, R.K. - Acta Met., 14, 1489 / 1495, 1966

2) Ahmed, M. & Potter, D.I. - Acta Met., 33, 2221, 1985.

3) Ansell, G.S. & Lenel, F.V. - Acta Met., 8, 612, 1960.

4) Ashby, M. - Z. Metalk., 55, 5, 1964.

5) Ashby, M.F. - Acta Met., 14, 679, 1966.

6) Bakhru, H., Gibson, W., Burr, C., Kumnick, A.J. & Welsch, G.E. - Nuc. Inst. Meth., 182/183, 959, 1981.

7) Broom, T.T. & Ham, R.K. - Proc. Royal. Soc. A, 251, 186, 1959

8) Chou, Y.T. - Phys. Stat. Solid., 17, 509, 1966

9) Coffin, L.F. - Trans. ASME, 76, 923, 1954.

10) Conners, G.H. - Int. J. Eng. Sci., 5, 25, 1967.

11) De Jonghe, L.C. & Greenfield, I.G. - Acta Met., 17, 1411, 1969.

12) Ebeling, R. & Ashby, M.F. - Phil. Mag., 13, 805, 1966

13) Ewing, J.A. & Humfrey, J.C.W. - Phil. Trans. Soc. A, 200, 241, 1902.

14) Finney, J.M. & Laird, C. - Phil. Mag., 31, 339, 1975

15) Fisher, J.C., Hart, E.W. & Pry, R.H. - Acta Met., 1, 336, 1953.

16) Follstaedt, D.M. - Nuc. Inst. Meth., B 7/8, 11, 1985.

17) Friedel, J. - "Dislocations", Pergamon Press, 1964.

18) Greenfield, I.G. - J. Sci. Indus. Res., 32, 521, 1973.

19) Greenfield, I.G. & Purohit, A. - Mat. Sci. Eng., 46, 89, 1980.

20) Grummon, D.S. - Doctoral Thesis, U. of Mich., 1986.

21) Grummon, D.S., Jones, J.W., Meridon, J.M., Was, G.S. & Rehn, L. - Nuc. Inst. Meth., B 19/20, 227, 1987.

22) Grummon, D.S., Jones, J.W. & Was, G.S.
- Met. Trans., 19A, 2775, Nov., 1988.

23) Hagg, G. - Z. Phys. Chem., B12, 33, 1931.

24) Head, A.K. - Proc. Royal Soc., B, 66, 793, 1953.

25) Heimendahl, M.V. & Thomas, G.
- Trans. AIME, 230, 1520, 1964.

26) Helgeland, O. - J. Inst. Met. , 93, 570, 1965.

27) Hellan, K. - "Intro. Fracture Mech.", Mcgraw-Hill, 1984

28) Hirsch, P.B. & Humphreys, F.J.
- Proc. Royal. Soc., A, 318, 45, 1970.

29) Hohmuth, K., Rauschenbach, B., Kolitsch, A. & Richter, E. - Nuc. Inst. Meth., 209 / 210, 249, 1983.

30) Hohmuth, K., Richter, E., Rauschenbach, B. & Blochwitz, C. - Mat. Sci. Eng., 69, 191, 1985.

31) Inman, M.C., Zwilsky, K.M. & Boone, D.H.
- Trans. ASM, 57, 701, 1964.

32) Jata, K.V. & Starke, E.A. - J. Metals, 23, Aug., 1983.

33) Jones, R.L. & Kelly, A.
- "Oxide Disp. Strength.", Gordon & Breach, 229, 1968

34) Jones, J.W. & Morrison, D. - General abstract session, TMS-AIME Fall Meeting, Cincinnatti, Sept. 1987.

35) Kelly, A. & Nicholson, R.B.
- Prog. Mat. Sci., 10, 1964.

36) Kimura, T. - Trans. Japan Inst. Met., 6, 217, 1965.

37) Koehler, J.S. - Phys. Rev., 60, 397, 1941.

38) Kujore, A., Chakraborty, S.B., Starke, E.A. & Legg, K.O. - Proc. Symp. Mat. Res. Soc.; Preece & Hirvonen, AIME, 132, 1980.

39) Kupcis, O.A., Ramaswami, B. & Woo, O.T.
- Acta Met., 21, 1131, 1973.

40) Laird, C., Langelo, V.J., Hollrah, M., Yang,N.C. & De La Veaux, R. - Mat. Sci. Eng., 32, 137, 1978.

41) Lauffer, E.E. & Roberts, W.N. - Phil. Mag., 14, 65, 1966

42) Leverant, G.R. - Trans. AIME, 239, 1992, 1967.

43) Leverant, G.R. & Sullivan, C.P.
- Trans. AIME, 242, 2347, 1968.

44) Manson, S.S. - Nat. Adv. Aero., Tech. note, 2933, 1954.

45) Mendez, J., Violan, P. & Villain, J.P.
- Scripta Met., 16, 179, 1982.

46) Mendez, J., Violan, P. & Denanot, M.F.
- Nuc. Inst. Meth., B 19/20, 232, 1987.

47) Meyers, C. & Grummon, D.S.
- General abstract session, TMS-AIME fall meeting, Sept. 1988.

48) Mori, T. & Mura, T. - Mat. Sci. Eng., 26, 89, 1976.

49) Mughrabi, H. - Mat. Sci. Eng., 33, 207, 1978.

50) Mughrabi, H. & Wang, R.
- "Defects, fracture & fatigue", Eds. Nijhoff, 15, 1982

51) Orowan, E. - Proc. Symp. on Internal Stresses in metals and alloys, Inst. Met., London, 451, 1948.

52) Palmer, I.G. & Smith, G.C.
-"Oxide Disp. Strength", Gordon & Breach, 47, 253, 1966

53) Peterson, R.E. - "Stress conc. factors", John Wiley, 34, 1974.

54) Sleeswyk, A.W., Kok, H.J.G. & Boom, G.
- Scripta Met., 14, 919, 1980.

55) Steiner, D. & Gerold, V. - Mat. Sci. Eng., 84, 77, 1986

56) Tomkins, B. - Phil. Mag., 1041, 1968.

57) Vardiman, R.G. & Kant, R.A.
- J. Appl. Phys., 53, 1, 690, 1982.

58) Vardiman, R.G. & Cox, J.E. - Acta Met., 33, 2033, 1985

59) Vogel, W., Wilhelm, M. & Gerold, V.
- Acta Met., 30, 21, 1982.

60) Wang, J.J., Welsch, G., Bakhru, H., Mashayekhi, A. & Gibson, W. - Nuc. Inst. Meth., B 7/8, 228, 1985.

61) Watt, D.F., Embury, J.D. & Ham, R.K.
- Phil. Mag., 17, 1991, 1968

62) Wells, C.H. & Sullivan, C.P. - Trans. ASM, 57, 841,1964

63) Wilhelm, M. - Mat. Sci. Eng., 48, 91, 1981.